Role of Co_3O_4 Nanoparticles on Impedance Properties of CuTl-1223 Superconductor

by:

Badshah Amin
(366-FBAS/MSPHY/F15)

Supervisor:

Dr. Muhammad Mumtaz
Associate Professor
Department of Physics, FBAS,
IIUI, Islamabad

Department of Physics
Faculty of Basic and Applied Sciences
International Islamic University, Islamabad

(2017)

Nanotechnology.
Nanoparticles.
X-Ray diffraction.

Role ofCo_3O_4Nanoparticles on Impedance Properties of CuTl-1223 Superconductor

by:

Badshah Amin

(366-FBAS/MSPHY/F15)

This Thesis submitted to Department of Physics International Islamic University Islamabad, for the award of degree of
MS Physics.

CHAIRMAN
DEPT. OF PHYSICS
International Islamic University
Islamabad

Chairman, Department of Physics
International Islamic University, Islamabad

Dean Faculty of Basic and Applied Science
International Islamic University, Islamabad

Department of Physics
Faculty of Basic and Applied Sciences
International Islamic University, Islamabad

Final Approval

It is certified that the work presented in this thesis titled **"Role of Co_3O_4 Nanoparticles on Impedance Properties of CuTl-1223 Superconductor"** by **Badshah Amin**, Reg. No,366-FBAS/ MSPHY/ F15 is of sufficient standard in scope and quality for the award of degree of MS Physics from Department of Physics, FBAS, International Islamic University, Islamabad, Pakistan.

Viva Voce Committee

Chairman (Physics) _____ (Prof. Dr. Mushtaq Ahmad).

Supervisor _____

External Examiner _____

Internal Examiner _____

DEDICATED

to

My beloved

Mother

Father

Wife

and

My

Respected teachers

Declaration

I **Badshah Amin** Reg. No 366-FBAS/MSPHY/F15, student of MS Physics (2015-2017), here declare that the matter printed in the thesis titled "**Role of Co_3O_4 Nanoparticles on Impedance Properties of CuTl-1223 Superconductor**" is my own work and has not been published or submitted as research work or thesis in any form in any other university or institute in Pakistan or aboard.

Badshah Amin

Dated: 3-10-2017

(366-FBAS/MSPH/F15)

Forwarding Sheet by Research Supervisor

The thesis titled **"Role of Co_3O_4 Nanoparticles on Impedance Properties of CuTl-1223 Superconductor"** submitted by **Badshah Amin** in partial fulfillment of MS degree in Physics has been completed under my guidance and supervision. I am satisfied with the quality of student's research work and allow him to submit this thesis for further process to graduate with Master of Science degree from Department of Physics, FBAS, as per IIUI rules and regulations.

Dated: 04-10-2017

Dr. Muhammad Mumtaz
Assistant Professor
Department of Physics IIUI

Acknowledgment

First, I owe my deepest gratitude to **Allah** Almighty for all of his countless blessings. I offer my humblest words of thanks to HIS most noble messenger **Hazrat Muhammad (P.B.U.H),** who is forever, a torch of guidance and knowledge for all humanity. By virtue of his blessings today I am able to carry out our research work and present it.

I would like to acknowledge the worth mentioning supervision of **Dr. Muhammad Mumatz** who guided me and supported me during my whole research work. Without his guidance it was not possible for me to complete my MS (physics). Almighty **Allah** blessed him in every part of life.

I especially want to acknowledge my brothers **Qr. Muhammad yaqoob, Qr. Ajab khan, Qr. Bekhte Amin, Waheed-ul-Allah**, and my **wife** for their encouragement, support and confidence on me. During my education career their personality will remain the role model for me. Finally I am thankful to my **parents** and **sisters** for their love, care and support in my life, which has been directly encouraging me for my study. My parents' prayers have always been a big support in solving my problems. Allah may bless my parents and family with long life, health and happiness. I also pay special thanks to **Liquat Ali** and **Abrar Khan** who supported me during my research work. It was impossible to complete this work without their efforts.

Badshah Amin.

Table of Contents

Abstract xiii

CHAPTER 1 ..... **Error! Bookmark not defined.**

Introduction 1

1.1 Theoretical Background 1

1.1.1 Conduction in metals 1

1.1.2 Discovery of Superconductivity 3

1.2 Zero Resistivity 4

1.2.2 Phase Transition Temperature 5

1.2.3 The Isotope Effect 5

1.3 The Critical Parameters of Superconductors 6

1.3.1 The Critical Temperature ($\mathbf{T_c}$) 6

1.3.2 The Critical Magnetic Field ($\mathbf{H_c}$) 6

1.3.3 The Critical Current Density 7

1.4 The Meissner Effect 8

1.5 The Perfect Diamagnetism 10

1.6 Types of Superconductors 12

1.6.1 Type-I Superconductors 12

1.6.2 Type-II Superconductors 13

1.7 The Mixed State 14

1.8 The A-15 Type Superconductors 15

1.9 The London Theory 16

1.10 Penetration Depth, Coherence Length and Ginzburg-Landau Constant 17

1.10.1 Penetration Depth 17

1.10.2 Coherence Length 18

1.10.3 The Ginzburg-Landau Constant 19

1.11 The BCS Theory of Superconductivity 19

1.12 Complex Impedance Spectroscopy 19

1.12.1 Brief Histry of Impedance 20

CHAPTER 2 23

Literature Review 23
2.1 Literature Review 23
CHAPTER 3 28
Synthesis and Characterization Techniques 28
3.1 Synthesis of Nanoparticles 28
3.1.1 Chemical Methods (Bottom up approach) 28
3.1.2 Physical Method (Top down approach) 28
3.2 Synthesis of Co_3O_4 Nanoparticles 29
3.3 Synthesis of Precusor $Cu_{0.5}Ba_2Ca_2Cu_3O_{10-\delta}$ 29
3.4. Characterizations 31
3.4.1 X-Ray Diffraction Analysis 31
3.4.1.1 Bragg's Law 31
3.4.1.2 Debye Scherrer Equation 32
3.4.1.3 Diffratometer 33
3.5 LCR (Inductance, Capacitance and Reactance) meter 34
3.5.1 Handheld LCR meter ..... .35
3.5.2 Bench top LCR meter 35
3.6 SEM (Scanning Electron Microscope) 35
3.6.1 Formation of Image 36
3.6.2 Back Scattered Electrons 37
3.6.3 Secondary Electrons 37
3.6.4 Auger Electrons 37
3.7 R-T Measurement by Four Probe Method 38
CHAPTER 4 40
Results and Discussion 40
4.1 XRD Analysis 40
4.2 R-T Measurements 41
4.3 Impedance Analysis 42
4.4 Conclusions 49

References 50

List of Figures

Figure 1.1: The schematic diagram of resistivity verses temperature for pure and impure metal.3

Figure 1.2: Schematic diagram of resistance verses temperature of mercury 3

Figure1.3: The schematic diagram of normal state, critical temperature, T_c, and superconducting state 4

Figure 1.4: The variation of $\mathbf{H_c}$ with temperature 7

Figure 1.5: The diagram of the critical parameters of superconductor 8

Figure 1.6: The schematic diagram of the meissner effect 8

Figure 1.7: The schematic diagram of the Meissner effect 10

Figure 1.8 The diagram of magnetization versus applied magnetic field of diamagnetic material.....11

Figure 1.9: The response of diamagnetic material to applied magnetic field 12

Figure 1.10: The diagram of type I superconductors 13

Figure 1.11: The diagram of type II superconductors 14

Figure 1.12: The schematic diagram of type II superconductor, below $\mathbf{H_{c1}}$ is the Meissner state, above $\mathbf{H_{c2}}$ is the normal state, and between $\mathbf{H_{c1}}$ and $\mathbf{H_{c2}}$ is the mixed state 14

Figure 1.13: The schematic diagram of vortices in mixed state 15

Figure 1.14: Magnetic field penetrates into a superconducting specimen, indicating the penetration depth 17

Figure 1.15: The schematic diagram of the cooper pair formation 18

Figure 1.16: Symbolic representation of polycrystalline material and its complex impedance response 20

Figure1.17: The Argand diagram of complex impedance 21

Figure 3.1: The flow chart of synthesis of Co_3O_4 nanoparticles 39

Figure 3.2: The flow chart of the synthesis of $Cu_{0.5}Ba_2Ca_2Cu_3O_{10-\delta}$ 30

Figure 3.3: The flow chart of the preparation of composite.....30

Figure 3.4: The diagram of Bragg's Law and diffraction of x-rays from planes of a crystal 32

Figure 3.5: The schematic diagram for calculation of grain size..... 33

Figure 3.6: Diagram of x-ray Diffractometer.....34

Figure 3.7:The schematic diagram of LCR meter 34

Figure 3.8: Diagram of handheld LCR meter 35

Figure 3.9: SEM diagram..... 36

Figure 3.10: The diagram of auger effect 38

Figure 3.11: The diagram of two and four probe technique 39

Figure 4.1: XRD pattern of cobalt oxide (Co_3O_4)nanoparticles 40

Figure 4.2: The XRD patterns of polycrystalline sample of ((Co_3O_4)$_x$/CuTl-1223 nanoparticles superconductor composites) with x= 0 and 1.0 wt. %.....41

Figure 4.3: Resistivity as a function of temperature of polycrystalline sample {(Co_3O_4)$_x$/CuTl-1223 nanoparticles superconductor composites} with x= 0.0, 0.25, 0.50, and 1.00 wt.%.....42

Figure.4.4: (a-d): The temperature dependence of complex impedance plots of polycrystalline sample [$(Co_3O_4)_x$/CuTl-1223 nanoparticles-superconductor composites} with x= 0.0, 0.5, 1.0, and 2.0 wt. % in the frequency range (40 Hz – 10 MHz).....43

Figure.4.5: Activation energy of grains and grain-boundaries of the sample {$(\mathbf{Co_3O_4})_x$/CuTl-1223 nanoparticles-superconductor composites} with x= 0.0, 0.5, 1.0, and 2.0 wt. %..... 45

Figure 4.6: The real part of impedance ($\mathbf{Z'}$) of sample ($(\mathbf{Co_3O_4})_x$/CuTl-1223 (x= 0.0, 0.5, 1.0, and 2.0 wt. %) nanoparticles-superconductor composites) in frequency range (40 Hz – 10 MHz) at various temperatures (83 K – 243 K)..... 46

Figure 4.7: shows the imaginary part of complex impedance ($\mathbf{Z''}$) of the sample {$(\mathbf{Co_3O_4})_x$ /CuTl-1223 (x= 0, 0.5, 1 and 2 wt. %) nanoparticles superconductor composites} in frequency range (40 Hz – 10 MHz) at various temperatures (83K – 243K). 47

Figure 4.8:`Show AC conductivity of the sample ($(\mathbf{Co_3O_4})_x$ /CuTl-1223 (x= 0, 0.5, 1 and 2 wt. %) nanoparticles superconductor composites) in frequency range (40 Hz – 10 MHz) at various temperatures (83K – 243K). 48

TABLES

Table 1.2.1: Resistivity Table of Different materials 4

Abstract

The polycrystalline material $(Co_3O_4)_x$ /CuTl-1223; x= 0.0, 0.5, 1.0 and 2.0 wt. % was prepared with the help of sol gel and solid state reaction method respectively. X-ray diffraction analysis indicated that the samples have tetragonal crystal structure. Complex impedance spectroscopic method was used to study the electrical properties of the material in frequency ranges (40 Hz – 10 MHz) at various temperatures (83K – 243K). Complex impedance plots were suppressed with increase in temperature, which clearly confirmed the semiconducting nature of this material. The real part of impedance indicated that at low frequency, material has high resistance and at higher frequency the resistance of the material was decreased due to space charge polarization. The real part of impedance was also decreased with increasing concentration of Co_3O_4 nanoparticles which may be due to reduction of oxygen vacancies at grain boundaries. The imaginary part of impedance was shifted towards higher frequency with increasing concentration of Co_3O_4 nanoparticles, while with increase in temperature the height of the peaks was deceased.

Chapter 1
Introduction

This chapter includes brief discussion about metals, superconductors, basic experimental facts of superconductors, and impedance.

1.1 Theoretical Background

1.1.1 Conduction in metals

Metals are good electrical conductors in which current can easily flow with low resistance. Resistance of metals decreases with the decrease in temperature. The electrical current in a conductor is basically due to the motion of the conduction electrons. The core electrons are bound very tightly with the nucleus and form part of the metallic ion. Conduction electrons have high energy as compare with the core electrons. Metallic ions are immobile and only vibrate about their equilibrium position. Thus metallic crystal consists of immobile ions, conduction electrons, and other impurities. With the rise in temperature (above absolute zero) the atoms of the lattice vibrate with greater amplitude about the equilibrium position. The thermal vibrations of atoms, impurities, and defects scatter the conduction electrons which cause the resistance of the material. According to Drude theory the electrical conductivity of a metal is given as

$$\sigma = \frac{ne^2\tau}{m} \tag{1.1}$$

Where m is mass of the conduction electron, e is the charge on electron, and τ is the average lifetime of the conduction electron. Current density can be written as.

$$\mathbf{j} = \sigma\boldsymbol{\varepsilon} \tag{1.2}$$

Where **j**: current density, and $\boldsymbol{\varepsilon}$: is the external electric field. The reciprocal of resistivity is conductivity.

$$\rho = \frac{1}{\sigma} \tag{1.3}$$

Using the value of σ in equation (2) and readjusted

$$\boldsymbol{\varepsilon} = \rho\mathbf{j} \tag{1.4}$$

In term of ρ equation (1.1) can be written as

$$\rho = \frac{m\tau^{-1}}{ne^2} \tag{1.5}$$

Equation (1.5) shows that resistivity is proportional to τ^{-1}(scattering rate) of the conduction electrons.

In metals there are three main types of interactions,(i) electrons interact with electrons (ii) electrons interact with phonons and (iii) scattering by impurities. All these three types of interaction independent, so the total scattering rate can be written as

$$\tau_{total}^{-1} = \tau_{el-el}^{-1} + \tau_{el-ph}^{-1} + \tau_{imp}^{-1} \tag{1.6}$$

Put the value of τ_{total}^{-1} in equation (1.5) we get

$$\rho = \frac{m}{ne^2}(\tau_{el-el}^{-1} + \tau_{el-ph}^{-1} + \tau_{imp}^{-1}) \tag{1.7}$$

Scattering by impurity (τ_{imp}^{-1}) does not depend upon temperature, the interaction of electron with electron (τ_{el-el}^{-1}) is proportional toT^2 while electron phonon interaction (τ_{el-ph}^{-1}) is proportional to T^5. The resistivity of a metal can be written as

$$\rho = \rho_0 + aT^2 + bT^5 + \ldots \tag{1.8}$$

Where

T: lowest temperature, a, and b are constants.

When temperature of the metal reduces, the vibration of atoms also decreases as a result the scattering of electrons decreases. For ideal pure and perfect metal, where the motion of electrons only opposes by vibrations of the atoms, the resistivity becomes zero as temperature of the metal decrease to zero Kelvin (0 K). This is not a phenomenon of superconductivity. A pure metal always contain some impurities. The conduction electrons in metals are scattered by thermal vibrations of atoms and impurities. Scattering by impurities is independent of temperature. The residual resistivity (ρ_0) remain even at the lowest possible temperatures as shown in Fig.1.1 [1-2].

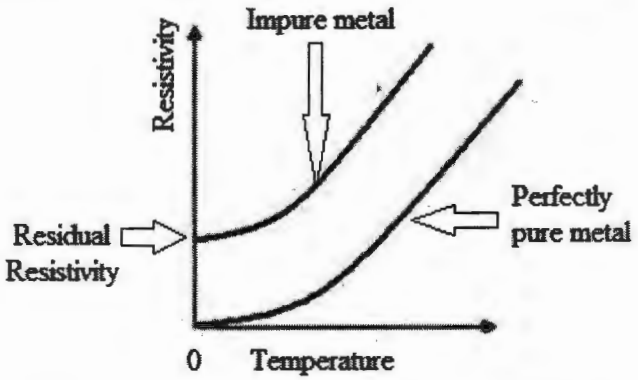

Fig.1.1: The graph of resistivity verses temperature for pure and impure metal [1].

1.1.2 Discovery of Superconductivity

Heike Kammerlingh Onnes was the first scientist who experimentally worked on the Drude model. He performed a number of experiments for the verification of Drude model. The first experiment on the samples of platinum and gold were agreed with Drude theory. After that H. Kammerlingh Onnes work on mercury. Since mercury is a pure metal with no impurity. He observed that as temperarure of mercury decreases resistance also decreass linearly and finally at a temperature about 4.2 K resistance of mercury completely vanish, as shown in Fig. 1.2. Those materials which completely losses their resistance at a certain temperature are called superconductors and this phenomenon is called superconductivity [2].

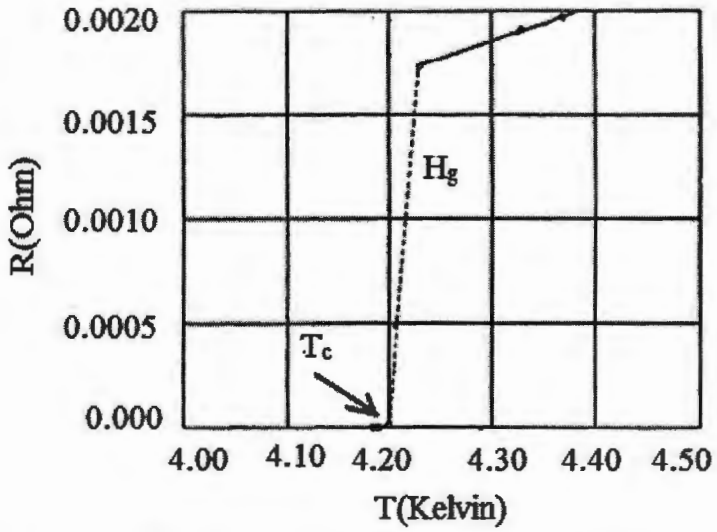

Fig.1.2: Schematic diagram of resistance verses temperature of mercury [4].

1.2 Zero Resistivity

In superconductors the resistivity (ρ) completely vanish and conductivity become infinite below certain transition temperature also called the critical temperature T_c. Above the transition temperature material in the normal state and conduction through the material is only due to conduction electrons; blow the transition temperature the material in the superconducting state. In superconductor electric field always zero, and current density, $\boldsymbol{j}$ has a finite value. So in superconducting materials current always flow without electric field. Normal state and superconducting state is shown in Fig.1.3. Normal state and superconducting state have different properties.

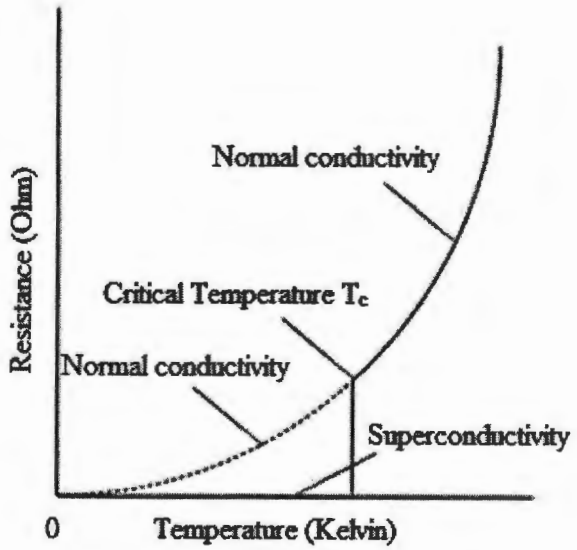

Fig.1.3: The schematic diagram of normal state, critical temperature, T_c and superconducting state [5].

1.2.1 Resistivity Table of Different materials

Materials	Resistivity, ρ (Ωm)
1. Superconductors	Zero
2. Metals	$10^{-8}\ \Omega m$
3. Semiconductors	Vary
4. Insulators	$10^{16}\ \Omega m$

1.2.2 Phase Transition Temperature

The phase transition temperature can be define as "the temperature at which a superconducting material completely loss their resistance" is known as the thermodynamic phase transition temperature or the critical temperature, it is denoted by T_c. The value of critical temperature is usually not sensitive to a minute amount of impurities, although magnetic impurities can reduce the value of critical temperature. In case of ferromagnetic material, in which the spins of the electrons are parallel aligned to each other, is not usually compatible with superconductivity. Elemental superconductors have very low transition temperature, in which the element niobium(Nb) has the highest critical temperature 9.2 K. A-15 type superconductors have relatively high transition temperature as compared with elemental superconductors. For example Nb_3Ge with T_c = 23 K and Nb_3Sn with T_c = 18 K. Cuprate superconductors have the highest thermodynamic phase transition temperatures. For example $HgBa_2Ca_2Cu_3O_{8+\delta}$ with T_c = 135 K at room temperature, and under the condition of high pressure its T_c rising to 165 K. All pure metals are not superconductors, such as copper, gold and silver, the main reason is the low interaction between electrons and phonons which prevent them from superconductivity [6].

1.2.3 Isotope Effect

Isotope can be defined as "The atoms of an element which have an equal number of protons due different number of neutrons" is called an isotope. Isotopes of an element have same electronic structure and chemical properties but different physical properties.

The critical temperature,T_c depend upon the mass of the isotope. The relation between mass of an isotope (M) and the critical temperature, T_c is given as

$$T_c \propto \frac{1}{\sqrt{M}} \tag{1.9}$$

Equation (1.9) shows that critical temperature (T_c) is inversely proportional to $\sqrt{M}$. Therefore a sample compose of lighter isotopic mass, M have higher transition temperature, T_c than a sample which compose of heavier isotopic mass. There are certain elements which have zero isotope effect such as Zirconium (Zr) and Ruthenium(Ru), while metals Molybdenum (Mo) and Osmium (Os) shows a reduce effect [7-8].

1.3 Critical Parameters of Superconductors

The critical parameters of superconductors are current density ($\mathbf{j_c}$), magnetic field ($\mathbf{H_c}$), and temperature (T_c).

1.3.1 Critical Temperature (T_c)

Critical temperature is basically a certain temperature at which a superconducting material completely losses their resistance is called the critical temperature. Every material has a unique transition temperature. As the material cool below the transition temperature the conduction electrons form the bound pair of electrons, which in simple words called the Cooper pair, and condensed at the Fermi surface in the form of bosons with a spin zero. When temperature of the superconducting material increases, Cooper pairs break down the bound state energy release, and finally above T_c the material completely transform from superconducting state to normal state [6].

1.3.2 Critical Magnetic Field (H_c)

A very strong external magnetic field (applied magnetic field) can easily destroy the superconducting state of a material. The minimum value of the external magnetic field at which a material transform from superconducting state to normal state is called the critical magnetic field $\mathbf{H}_c(T)$. The critical magnetic field increase as temperature decrease, and reaches a maximum value $\mathbf{H}_c(0) = \mathbf{H}_0$ as T→ 0. It is clear from the following equation that the value of critical magnetic field becomes zero at $T = T_c$

$$H_c = H_0\left[1 - \left(\frac{T}{T_c}\right)^2\right] \tag{1.10}$$

The above relation also known as the Gorter-Casimir equation [9]. It is also clear from the Fig.1.4 as we decrease temperature below T_c ($T < T_c$) the value of the critical field, $\mathbf{H}_c$ increase, and finally the value of $\mathbf{H}_c$ becomes maximum at $T = 0$ [6].

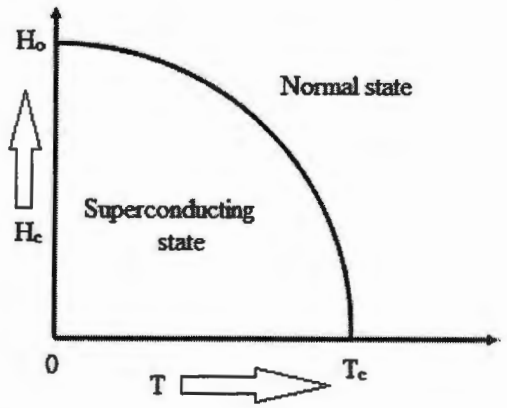

Fig.1.4: The variation of $\mathbf{H}_c$ with temperature [6].

1.3.3 Critical Current Density

The current density, **j** in simple words is the current per unit area; its unit is ampere per meter. All superconductors have three critical parameters that is critical current, magnetic field, and current density ($\mathbf{j_c}$). In case of superconductors the critical current density must have an upper limit at which superconductivity is completely losses, and material transform to normal state [10].

The critical current density of type I superconductors is very low as compared with the critical current density of type II superconductors, that is the reason of limited application of type I superconductors as compared to type II superconductors.

The relationship of the three critical parameters that is critical magnetic field, critical current density and critical temperature is sketch in the following Fig.1.5. This figure is also called as THJ diagram [11].The inner surface of the figure represents the superconducting state, while the outer surface represents the normal state [6].

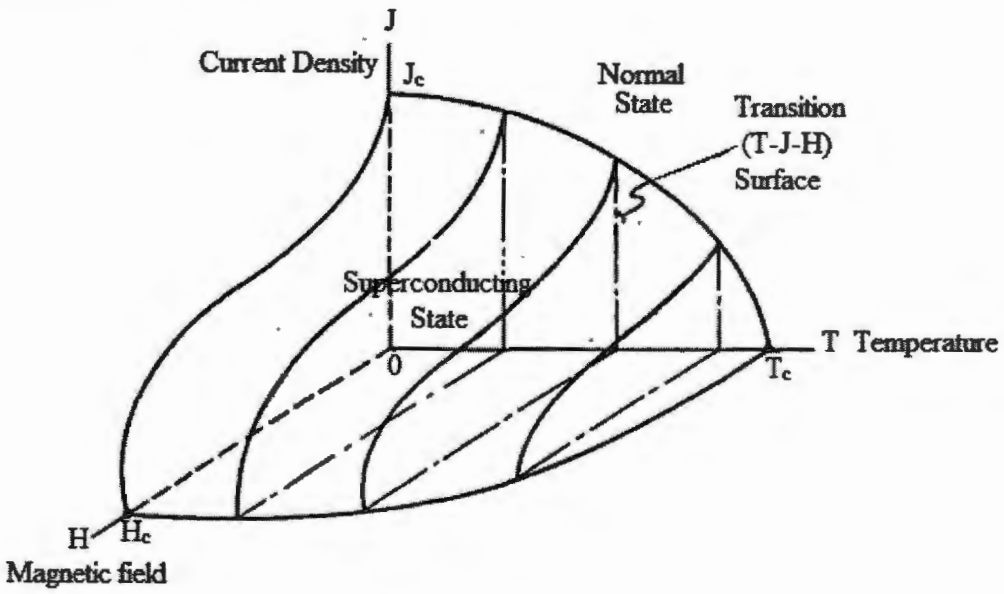

Fig.1.5: The schematic diagram of the parameters of the superconductor [6].

1.4 Meissner Effect

Whenever a superconducting material is placed inside a weak external magnetic field (that is field of a solenoid or permanent magnet) below its superconducting transition temperature, then it completely expels the magnetic lines of force from its interior as shown in Fig.1.6. In 1933 this phenomenon was discovered by Meissner and Ochsenfeld.

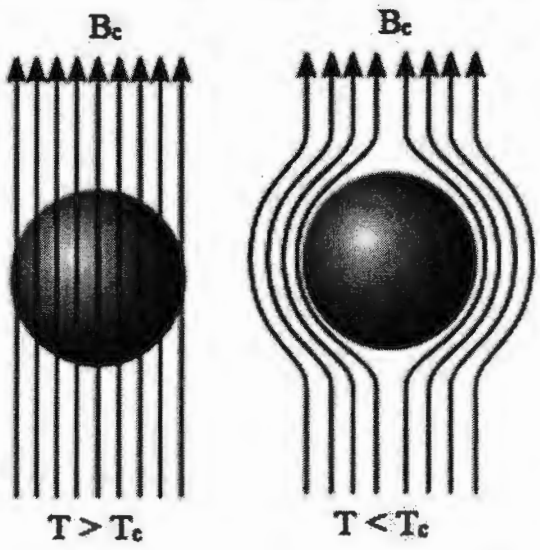

Fig.1.6: The schematic diagram of the Meissner effect [12]

Let us consider a sample initially in its normal state $(\text{i.e.}\, T > T_c)$ and zero applied magnetic field $(\boldsymbol{B_{ext}} = 0)$ as given in left hand side of Fig. 1.7. If we first cool the sample below the critical temperature and then place it in a weak external magnetic field, magnetic lines of force do not penetrate the sample and as a result field inside the sample remain zero. By Maxwell equation

$$\nabla \times \boldsymbol{\varepsilon} = \frac{\partial \boldsymbol{B}}{\partial t} \tag{1.10}$$

Since $\varepsilon = 0$ at every point inside a superconductor, therefore equation (1.10) can be written as

$$\frac{\partial \boldsymbol{B}}{\partial t} = 0 \tag{1.11}$$

$$\int d\boldsymbol{B} = \int 0 dt \tag{1.12}$$

$$\boldsymbol{B} = 0 \tag{1.13}$$

Equation (1.13) shows that magnetic field inside the sample is zero.

Suppose we take the sample in its normal state $(i.e. T > T_c)$, and apply the external magnetic field, $\boldsymbol{B_{ext}}$.This time magnetic field easily penetrate through the sample as shown in the right side of Fig.1.7. Upon cooling the sample below the transition temperature, T_c the magnetic lines of forces again expels from inside the sample. From Fig.1.7 it is clear that we can reach the final state of the system, if we first cool the sample and then apply the magnetic field, or first apply field and then cool. So we define a superconductor as "a material which obeys the Meissner effect [2].

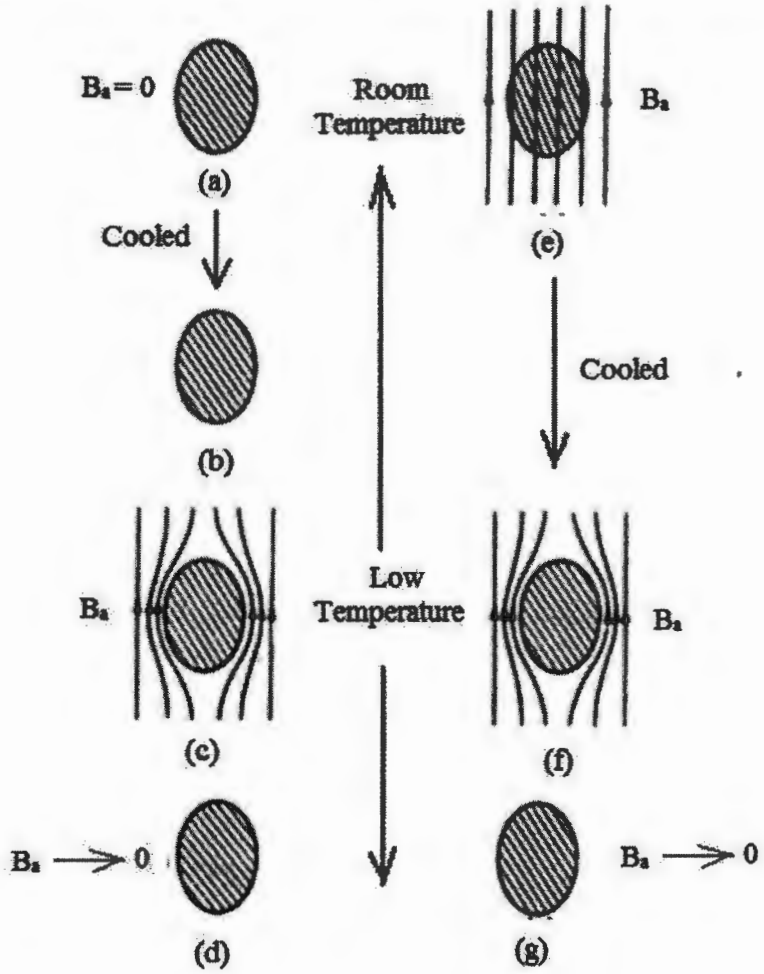

Fig.1.7: The schematic diagram of the Meissner effect [1].

1.5 The Perfect Diamagnetism

Those materials in which induce magnetization produces in a direction opposite to the applied magnetic field are called diamagnetic materials. Diamagnetic materials weakly repel in the magnetic field as shown in Fig.1.9, and have a negative magnetic susceptibility($\chi_m = -1$) as shown in Fig.1.8. Silver, gold, copper, silicon and alumina are the examples of diamagnetic materials at room temperature.

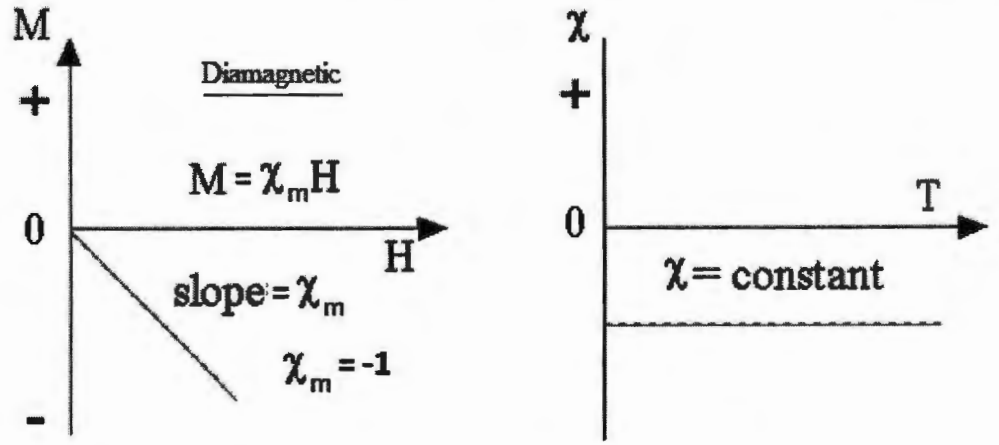

Fig.1.8: The diagram of magnetization versus applied magnetic field of diamagnetic material [13].

Let's suppose we have a sample of superconducting material below its transition temperature. When the sample is placed in a weak external magnetic field (i.e. solenoid, or a permanent magnet, etc) blow its critical temperature, T_c, the applied magnetic field induces currents which circulate on the surfaces of grains (i.e. on the surface of the sample). These surface currents produce its own magnetic field which is equal and opposite to the direction of an applied magnetic field. So as a result magnetic field ($\mathbf{B_{ext}} = 0$) inside the sample remains zero. These surface currents are also known as screening currents or persistent currents. The total current is given as

$$\mathbf{j} = \mathbf{j_{ext}} + \mathbf{j_{int}}. \tag{1.14}$$

Where $\mathbf{j}$ is the total current, $\mathbf{j_{ext}}$ is the external current (current passing in the coils of solenoid), and $\mathbf{j_{int}}$ is the current which circulate on the surface of the sample and which is responsible for the magnetization of the sample. Magnetization can be written in terms of $\mathbf{j_{int}}$

$$\nabla \times \boldsymbol{M} = \mathbf{j_{int}} \tag{1.15}$$

And

$$\nabla \times \boldsymbol{H} = \mathbf{j_{ext}} \tag{1.16}$$

The relation between **M**, **H**, and **B** is given as

$$\mathbf{B} = \mu_0(\mathbf{H} + \mathbf{M}) \tag{1.17}$$

As$\mathbf{B} = 0$ inside the sample, so equation (1.17) can be written as

$$\mathbf{M} = -\mathbf{H} \tag{1.18}$$

Magnetic susceptibility can be define as

$$\chi_m = \frac{\mathbf{M}}{\mathbf{H}} \tag{1.19}$$

Using equation (1.18) in (1.19) we get

$$\chi_m = -1 \tag{1.20}$$

Substances which have negative value of magnetic susceptibility are known as diamagnetic substances. Diamagnetic substances expel a part of the applied magnetic field and magnetize opposite to direction of applied magnetic field. In case of superconductors the external applied magnetic field is completely ejected, so superconductors are known as perfect diamagnetic [2].

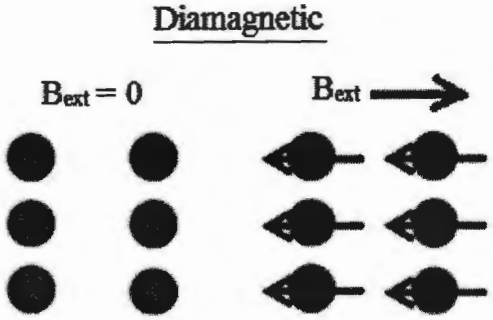

Fig.1.9: The response of diamagnetic material to applied magnetic field [14].

1.6 Types of Superconductors

On the bases of response to an applied magnetic field superconductors can be divided into two main types, that is type I and type II superconductors.

1.6.1 Type-I Superconductors

Superconductors which completely obey the Meissner Ochsenfeld effect is known as type I superconductors. It has a single critical field, $\mathbf{H_c}$. It is also known as soft superconductors due to their dramatic response to an applied magnetic field. The coherence length in type I superconductors is greater than the penetration depth ($i.e. \lambda < \xi$).Type-I superconductors have positive surface energy. In type-I superconductor magnetic field remains zero ($\mathbf{B} = 0$) inside the superconductor until superconductivity is destroyed, and sample transform from superconducting stat to normal stat. The field at which superconducting stat transform to normal stat is known as the critical field, $\mathbf{H_c}$. It is clear from Fig 1.10, that there is a linear relationship between $\boldsymbol{M}$ and $\mathbf{H}$ (i.e. $\mathbf{M} = -\mathbf{H}$) below$\mathbf{H_c}$, and above $\mathbf{H_c}$magnetization completely vanish. Examples of type-I are Al, Hg, Sn, Zn, Tl, etc [6].

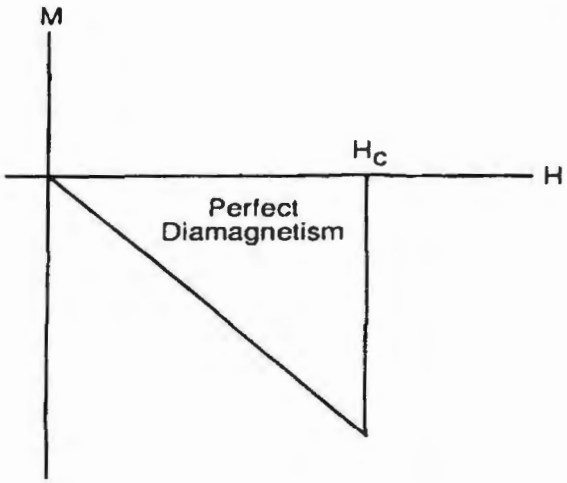

Fig.1.10: The diagram of type I superconductors [6].

1.6.2 Type- II superconductors

Superconductors which do not completely obey the Meissner Ochsenfeld effect are known as type II. It is also called hard superconductors. Type II superconductors consists of two critical fields, the lower critical field, $\mathbf{H_{c1}}$ and the upper critical field, $\mathbf{H_{c2}}$.The size of the coherence length in type II superconductor is less than the penetration depth $(i.e.\xi < \lambda)$. When the value of applied field, **H** is less than $\mathbf{H_{c1}}$than the Meissner Ochsenfeld effect obey, and magnetization follows the path $\mathbf{M} = -\mathbf{H}$ with $\mathbf{B} = 0$ inside the sample. But when the value of applied magnetic field exceeds than the lower critical field, $\mathbf{H_{c1}}$, the magnetic lines of forces start to penetrate the sample, and $\mathbf{B} \neq 0$, and magnetization reduces to zero. When the value of **H** further increases, the value of **B** also increases and finally at $\mathbf{H_{c2}}$ the superconducting stat completely destroy, and magnetization vanish, $\mathbf{M} = 0$ as shown in the Fig 1.11.Examples of type-II superconductor are cooperate superconductors and A-15 type superconductors [6].

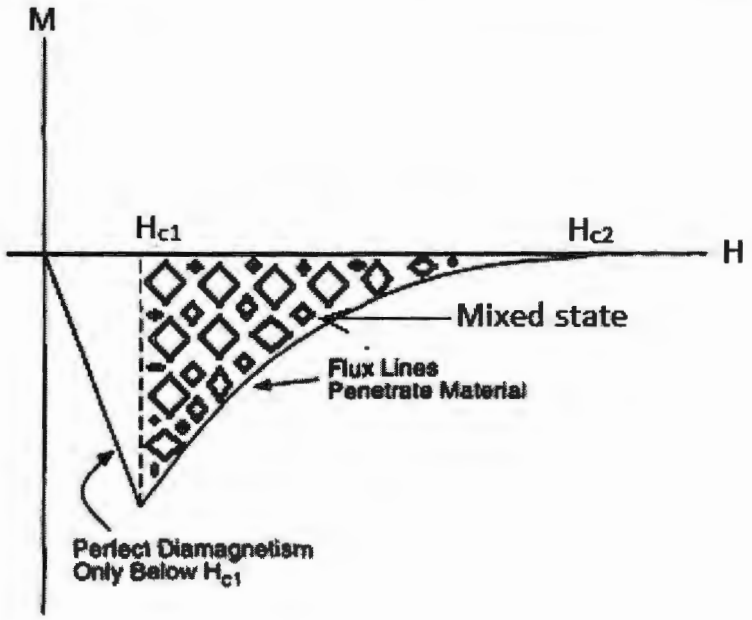

Fig.1.11: The diagram of type II superconductors [6].

1.7 Mixed State

In type II superconductors, the area between the lower critical field, $\mathbf{H_{c1}}$ and upper critical field, $\mathbf{H_{c2}}$ is called the mixed state or the Abrikosov state as shown in Fig.1.12. The mixed state was first explained by Abrikosov.

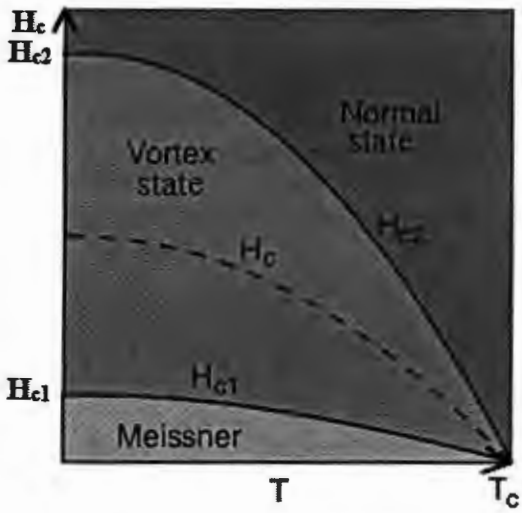

Fig.1.12: The schematic diagram of type II superconductor, below $\mathbf{H_{c1}}$ is the Meissner state, above $\mathbf{H_{c2}}$ is the normal state, and between $\mathbf{H_{c1}}$ and $\mathbf{H_{c2}}$ is the mixed state [2].

He stated that the external applied magnetic field can pass through the superconducting in the form of magnetic lines of force or flux tube, around the flux tube a circulating current is produce which is known as the supercurrent. These circulating currents (i.e. supercurrent) expel the magnetic field from the superconductor just outside the vortices. Type-II superconductors consist of natural defects such as impurities, grain-boundaries, voids and dislocations. Magnetic field can easily pass through these natural defects in the form of flux tube, which encircling by superconducting current. There are repulsive interactions between the cores of vertices such as between two solenoid or bar mar magnet. The vortices form a regular periodic lattice arrangement, either hexagonal or square form. This arrangement is usually called as the fluxon lattice. The magnetic flux through each vortex is$\phi_0 = h/2e$. The resistance in type-II superconductors is due to the motion of vortices [1-2].

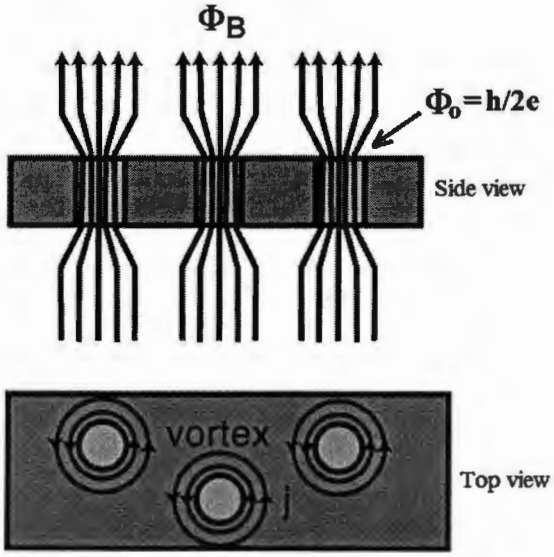

Fig.1.13: The schematic diagram of vortices in mixed state [2].

1.8 A-15 Type Superconductors

A-15 type superconductors were discovered in 1954. A large number of papers were published on this work [15]. The story of these compound start with the discovery of high critical temperature of Nb_3Sn and V_3Si [16-17].

The general formula of A-15 type superconductors is A_3B, where 'A' stand for transition element (i.e. Zr, Nb, Mo, W, Ta, Cr, Ti, V) and B represent either a non transition element (i.e. Sn, Pb, Sb, Bi, In, As, Ge, Ga, P, Si, Al) or transition elements (i.e. Au, Ir, Pt,

Os, Re, Rh, Pd, Ru, Co, Ni). The B atoms form a body centered cubic lattice (BCC), whereas A atoms situated on each face and form chains through the structure.

Before 1986, A-15 type superconductors were considered as the high critical temperature superconductors. The majority of the A-15 type binary compounds are superconductors, and at least fifteen of them have a transition temperature greater than 10 K. The properties of a superconductor strongly depend upon composition and atomic arrangement [18-19]. The best of A-15 type superconductor is Nb_3Ge with a thermodynamic phase transition temperature, T_c= 23 K, and Nb_3Sn with T_c= 18 K, which are use in industries for formation of superconducting coils for the purposes of high field generation.

1.9 The London Theory

The model of electricity could not explain the Meissner effect. In 1935, the Meissner effect was first time theoretically explained by F. London and H. London. In superconductors current flows without any resistance. In superconductors circulating currents produces its own magnetic field which cancels the applied magnetic field.

The London theory gives a relation between current density, $\boldsymbol{j}$inside the superconductor and magnetic vector potential:

$$\boldsymbol{j} = \frac{-1}{\mu_0 \lambda^2} \boldsymbol{A} \tag{1.21}$$

The above equation (1.21) is called the London equation. From here we use a lot of Maxwell's equation to get the final result. The relation between magnetic field and magnetic vector potential is given by$\boldsymbol{\nabla \times A = B}$.

Taking curl on both side of equation (1.21) we get

$$\boldsymbol{\nabla \times j} = \frac{-1}{\mu_0 \lambda^2} \boldsymbol{\nabla \times A} \tag{1.22}$$

Now put the value o f $\boldsymbol{B}$ in above equation

$$\boldsymbol{\nabla \times j} = \frac{-1}{\mu_0 \lambda^2} \boldsymbol{B} \tag{1.23}$$

From Maxwell's equations, we know that

$$\boldsymbol{\nabla \times B} = \mu_0 \boldsymbol{j} \tag{1.24}$$

Now taking the curl on both side of this equation we get

$$\boldsymbol{\nabla \times \nabla \times B} = \mu_0 \boldsymbol{\nabla \times j} \tag{1.25}$$

But

$$\nabla \times \nabla \times \boldsymbol{B} = \nabla(\nabla . \boldsymbol{B}) - \nabla^2 \boldsymbol{B} \tag{1.26}$$

From Maxwell's equations, $\nabla . \boldsymbol{B} = \mathbf{0}$, which reduce the above equation to

$$\nabla \times \nabla \times \boldsymbol{B} = -\nabla^2 \boldsymbol{B} \tag{1.27}$$

Now comparing equations (1.25) and (1.27), we have

$$-\nabla^2 \boldsymbol{B} = \mu_0 \nabla \times \boldsymbol{j} \tag{1.28}$$

Put the value of, $\nabla \times \boldsymbol{j}$ from equation (1.23) in equation (1.28), we get

$$\nabla^2 \boldsymbol{B} = \frac{1}{\lambda^2} \boldsymbol{B} \tag{1.29}$$

The only consistence solution to this equation is that, $\boldsymbol{B} = \mathbf{0}$ inside the superconductor, which confirm that the magnetic field is completely expels from inside the superconductor. The general solution of the above equation can be written as

$$\boldsymbol{B}(x) = \boldsymbol{B}_0 e^{(-x/\lambda)} \tag{1.30}$$

Where λ: London penetration depth and x: depth inside the superconductor [6, 20].

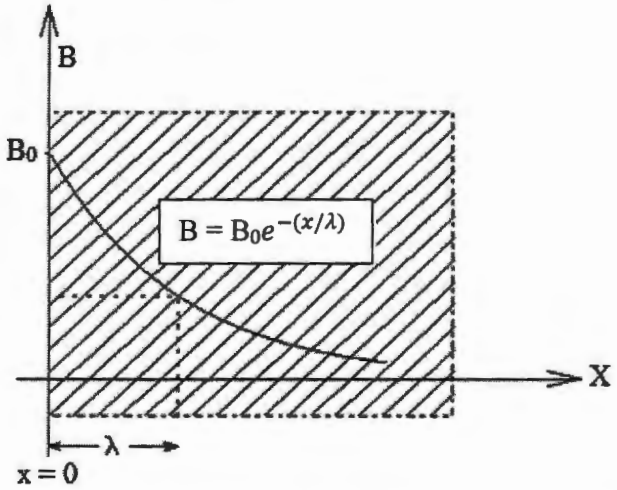

Fig.1.14: Magnetic field penetrates into a superconducting specimen, indicating the penetration depth [1]

1.1 0 Penetration Depth, Coherence Length and Ginzburg-Landau Constant

1.10 .1 Penetration depth

Penetration depth is the distance inside the surface of a superconductor at which an applied magnetic field becomes zero". It is denoted by λ and has the dimensions of length.

$$\lambda = \sqrt{\frac{m_e}{\mu_0 n_s e^2}} \tag{1.31}$$

Where

m_e: Effective mass of electrons

n_s: Density of superconductor electrons

e: Charge on electron

μ_0: Permeability of free space

1.10.2 Coherence Length

The bound pair of electrons in a superconductor is known as the Cooper pair as shown in Fig.1.15. The size of the Cooper pair is known as the Coherence length, and it is denoted by, ξ_0. The concept of coherence length was first given by Pippard [21-22]. Impurities in a sample basically increase the scattering of electrons, as a result both the mean free path and coherence length decrease. High temperature superconductors (Type-II) always consists of natural defects such as impurities, grain- boundaries, voids and dislocations, due to these defects the coherence length in type-II superconductor is smaller as compared to penetration depth ($\xi_0 < \lambda$). But in case of pure elemental superconductors $\lambda < \xi_0$.The relation of coherence length, ξ_0, energy gap, Δ, and Fermi velocity, V_F, is given by the following equation [1].

$$\xi_0 = \frac{\hbar V_F}{\pi \Delta} \tag{1.32}$$

Where

$\hbar$: Plank constant.

V_F : Fermi velocity

Δ : Energy gap.

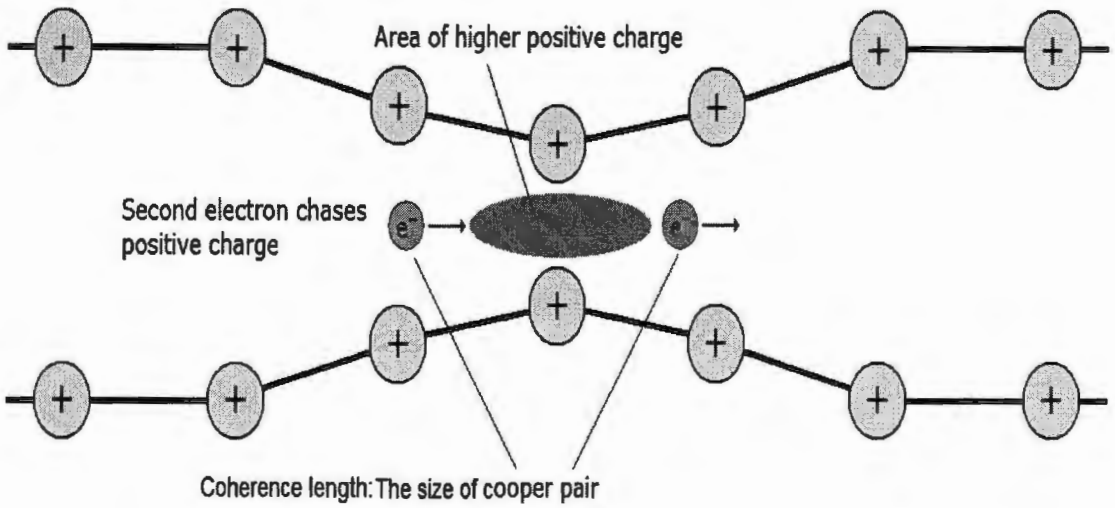

Fig.1.15: The schematic diagram of the cooper pair formation [23].

1.10.3 Ginzburg-Landau Constant

The Ginzburg- Landau constant is basically penetration depth (λ) divided by coherence length (ξ_0), and it is denoted by symbol,κ, and can be given as

$$\kappa = \frac{\lambda}{\xi_0} \tag{1.33}$$

The Ginzburg- Landau constant, κ, is the most important parameter of superconductor, because it can easily differentiate between type-I and type-II superconductor depending whether the value of Ginzburg-Landau constant, κ, greater or less than one [1].

1.11 BCS Theory of Superconductivity

In 1957, the first microscopic theory of superconductivity was put forward by three scientists J. Bardeen, L. Cooper and J. R. Schrieffer and called as the BCS theory of superconductivity. This theory successfully explains the Meissner effect, the zero resistivity and isotopic effect. BCS theory consists of three major insights:

(i) The effective force between electrons can be attractive in solid.

(ii) The electrons outside the Fermi surface form a bound pair, however weak the attractive.

(iii) Schrieffer form a many particles wave function, that is all the electrons makes bound pairs near the Fermi surface [2].

1.12 Complex Impedance Spectroscopy

Impedance spectroscopy is one of the powerful and an important method which is use to characterize the electrical behavior of a material. Polycrystalline material consists of grain and grain-boundaries as shown in Fig.1.16 that have different relaxation time (time constants). Impedance spectroscopic technique helps us to separate the contribution of grain and grain-boundaries in electrical properties of the polycrystalline material.

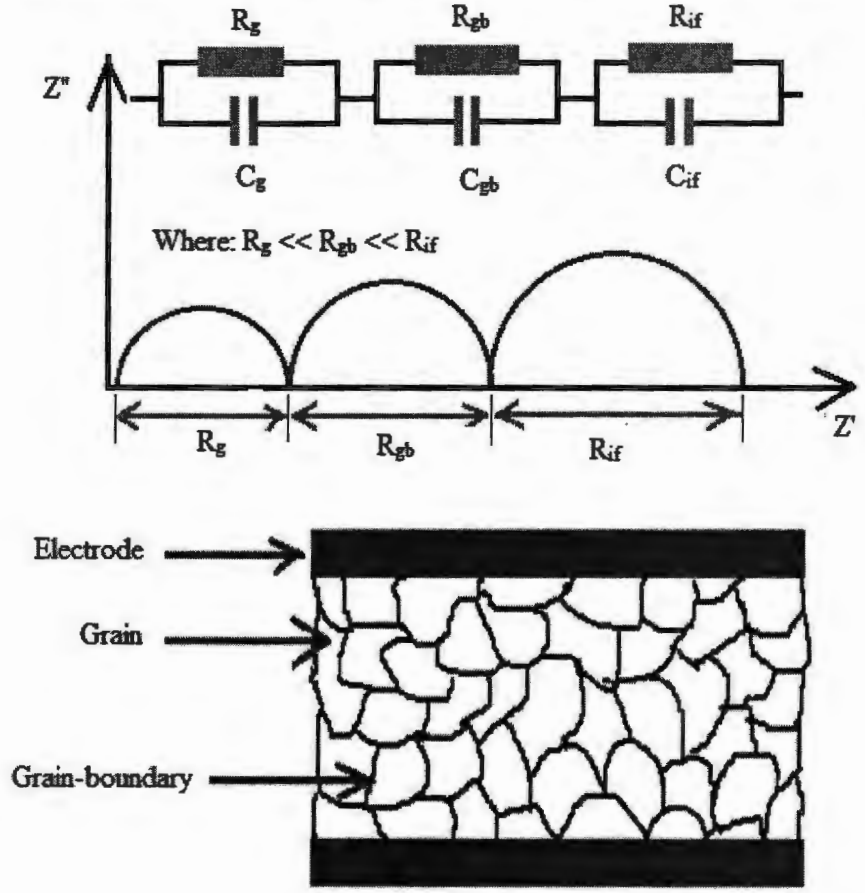

Fig. 1.16: Symbolic representation of polycrystalline material and its complex impedance response.

Where: Resistance of interface >> Resistance of grain boundary >> Resistance of grain Complex impedance spectroscopy is a very widely used and an important measurement technique applied in many field of research such as material science, medicine, electrochemistry and biology. It is use to study the dynamics of charges in bulk or interfacial regions of liquid or solid (i.e. amorphous, polycrystalline, and single crystal). A large number of materials can be easily characterize by impedance spectroscopy, it include semiconductors, ceramics, magnetic ferrite, polymers and membranes [24]

1.12.1 Brief History of Impedance

The idea of electrochemical impedance spectroscopy was first time given by Oliver Heaviside in 1880s. He developed the Laplace transformation, operational calculus, differentiation and integration. O. Heaviside defined complex impedance, admittance (the

inverse of impedance), reactance and operational impedance. C. P. Steinmetz and A. E. Kennelly modified the electrochemical impedance spectroscopy. These two scientists include a large number of vector diagrams and complex representation.

Impedance is usually denoted by Z, it is basically the resistance of a system (i.e. circuit or electronic component) when AC or DC current passing through it. Impedance is a complex quantity which has two components.

$$Z = Z' - jZ'' \tag{1.34}$$

Where $j = \sqrt{-1} = \exp(j\pi/2)$ is the imaginary number, which show the anticlockwise rotation by $\pi/2$ with respect to x axis. The real part of complex impedance (Z') is in the direction of x-axis and the imaginary part of complex impedance (Z'') is along the y-axis. Impedance basically is a vector quantity and can easily be resolved into two components as shown in Fig.1.17. From the figure it is clear that Z has two components that is

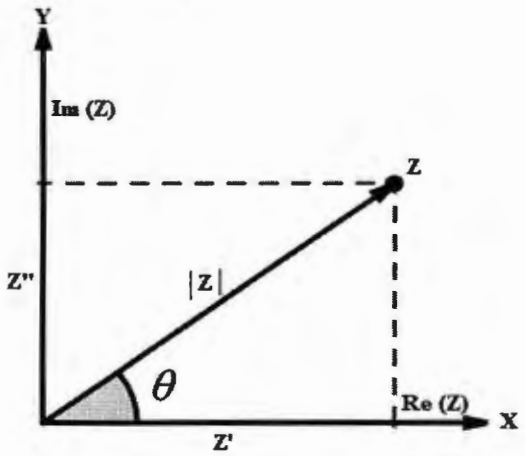

Fig.1.17: The diagram of complex impedance [25].

$$\text{Real part of } Z = Z' = (\text{magnitude of } Z)\cos\theta \tag{1.35}$$

$$\text{Imaginary part of } Z = Z'' = (\text{magnitude of } Z)\sin\theta \tag{1.36}$$

Where θ is the phase angle and is equal to

$$\theta = \tan^{-1}(Z''/Z') \tag{1.37}$$

Also

$$|Z| = \sqrt{(Z')^2 + (Z'')^2} \tag{1.38}$$

This is the magnitude of the complex plane, which is widely used in mathematics. In polar form impedance can be written as

$$Z = |Z|\, e^{j\theta} \tag{1.39}$$

Where

$$e^{j\theta} = \cos\theta + j\sin\theta \tag{1.40}$$

is the Euler equation.

Chapter No.2

Literature review

P. Khatri et al studied the impedance of the polycrystalline sample ($Ca_3Nb_2O_8$) as a function of frequency (10^2 Hz - 10^6 Hz) and temperatures (25 °C - 500 °C). The material was prepared by using solid state reaction technique. X-ray diffraction analysis was used for phase identification. Surface morphology of the material was studied with the help of SEM. The electrical properties of the sample were explained with the help of complex impedance spectroscopic technique. The impedance spectrum was depressed with increase in temperature which confirmed that sample has a semiconducting nature. Loss spectrum showed that (imaginary part of impedance versus frequency) the material has a temperature dependent relaxation processes. Complex modulus analysis indicated the existence of hopping processes in the sample [24].

Y. Wang et al explained the electrical properties of the polycrystalline material (1 - x) $BaTiO_3$ - x $BiYO_3$ ((1 – x) BT – xBY) (x= 0.2, 0.3) in frequency range (20 Hz – 2 MHz) at various temperature (250 ^{0}C – 400 ^{0}C). They used solid state reaction technique for preparation of the material. The dielectric analysis showed that the diffusive factor is about 1.8. Complex impedance and modulus analysis confirmed that there are two types of relaxation processes in the material. The imaginary part of impedance and modulus as a function of frequency at different temperatures confirmed the dielectric relaxation. The real part of complex impedance versus frequency and ac conductivity confirmed that the material has a semiconductor nature. The activation energy was about 0.98 eV [26].

S. Dash et al successfully explained the electrical properties (i.e. conductivity, impedance, and modulus) of the $(Bi_{0.6}K_{0.4})$ $(Fe_{0.6}Nb_{0.4})$ O_3 material in frequency range (1 kHz–1 MHz) at various temperatures (25 °C – 500 °C). The sample was prepared by solid state reaction technique. It was concluded from impedance spectrum that the conduction mechanism was basically due to contribution from both grains (290 ^{0}C) and grain-boundaries (T ≥ 300 ^{0}C). It was also noticed that dc conductivity follows the Arrhenius law, whereas ac conductivity obeys Joncher's power equation. The polarization versus electric field hysteresis loop confirmed the ferroelectric properties of the material with coercive field of 16.63kV/cm and remnant

polarization 1.027μC/cm^2. At room temperature the material showed weak ferromagnetism with coercive field of 0.211 kOe and remnant magnetization of 0.035emu/gm [27].

H. Singh et al explained the influence of $BaTiO_3$ on the ferroelectric, magnetic, and dielectric properties of the $BiFeO_3$ material. They synthesized the material by solid state reaction technique. The dielectric properties of the material were improved by $BaTiO_3$ substitution. In the dielectric constant an anomaly was observed near the Neel temperature. It was observed that material has semiconducting nature, grain and grain-boundary conduction at high temperatures and presence of polydispersive phenomenon in the material. The dielectric properties of $BiFeO_3$ at room temperature have useful for device application [28].

R. Muduli et al studied the electrical properties of $AgNbO_3$ (silver niobate) doped with X_2O_5 (X = Ta, Sb and V). solid state reaction method has been used for preparation of material. X-ray diffraction study confirmed that the sample has polycrystalline nature. SEM analysis was used for surface morphology. Complex impedance spectroscopy method was used to explain the contribution of grain and grain-boundaries in the conduction processes. A single relaxation processes was observed in both the imaginary part of complex modulus ($M^{''}$) and impedance ($Z^{''}$). It was concluded that metallic silver nano-particles have no effect on electric properties within the chosen frequency and temperature range [29].

D. K. Pradhan et al studied the impedance of layered perovsite ceramic oxide ($NaNdTiO_4$) as a function of frequency range at various temperatures. X-ray diffraction analysis was used for phase identification and SEM was used for surface morphology. Complex impedance analysis confirmed that material has semiconductor nature (that is negative temperature coefficient of resistance), grain-boundary effect above 500 ^{0}C, and different types of relaxation processes in the sample. The impedance behavior of the sample was explained with the help of brick layer model. It was also concluded that material has higher electrical conductivity at 500 ^{0}C as compared at low temperature [30].

S. A. Nedil'ko et al studied the electrical properties of Barium cuprate ($BaCuO_{2+\delta}$(δ = 0.25) in frequency range (10^2 Hz – 10^6 Hz) at different temperatures (453 K - 593 K). The sample was prepared by secondary induction heating. The electrical properties were studied by complex impedance spectroscopy method. It was concluded from complex impedance that barium cuprate was highly homogeneous, and the sample has relaxation processes within crystallites. It was

found that the conversion of 50% Cu^{2+} to Cu^{3+} decreased the energy barrier and increased the conductivity of the material. It was also concluded that the sample has semiconductor nature with activation energy about $E_{dc} = 0.29$ eV [31].

B. B. Mohanty et al studied the impedance of polycrystalline material ($Ba_5GdTi_3V_7O_{30}$) as a function of frequency (10^2 Hz - 10^6Hz) at various temperatures (300 °C – 500 °C). From complex impedance and complex modulus spectroscopy it was concluded that material has multi Debye type relaxation processes. The presence of peak in the loss spectrum indicates the existence of relaxation processes in the sample. The peaks in the loss spectrum were shifted towards the high frequency side and finally all the curves merge as a result of release of space charge. The complex impedance spectrum was depressed with the rise in temperature. It was concluded that the material has semiconducting nature and obey Arrhenius law [32].

Lily et al investigated the electrical properties of the material $(Na_{0.5}Bi_{0.5})(Zr_{0.25}Ti_{0.75})O_3$.The sample was synthesized by solid state reaction method. Impedance analysis showed the existence of intragrain and intergrain effects in the sample. It was found that the sample has multi-Debye type relaxation processes. The peaks in the loss spectrum were shifted towards higher frequency side with the rise in temperature. Complex impedance spectrum and conductivity analysis revealed that sample has a semiconducting nature. The frequency dependent ac conductivity at various temperatures showed that the conduction mechanism was thermally activated and obeys the power law [33].

P.S. Sahoo et al studied the impedance and modulus spectroscopy of $Ba_4SrSmTi_3V_7O_{30}$ ceramics material in frequency range (1 K Hz –1 MHz) at various temperatures (31 °C - 500 °C). The sample was synthesized with the help of solid state reaction method. X-ray diffraction was used for phase identification and complex impedance spectroscopy was used to characterize the electrical behavior of the sample. The impedance spectrum showed a non Debye type of dielectric relaxation processes. The impedance plots also revealed that the grain resistance decreased with the rise in temperature. The ac and dc conductivity analysis of $Ba_4SrSmTi_3V_7O_{30}$ revealed the semiconducting nature of the. It was also concluded that ac conductivity obey the power law and the conduction processes of the material was due to hopping of charge carriers across the grain boundaries [34].

Q. K. Muhammad et al studied the Structural, dielectric, and impedance of ZnO doped $BaZr_{0.15}Ti_{0.85}O_3$ (barium zirconium titanate) ceramics in frequency range (100 Hz - 1 MHz) at different temperatures (300 °C - 500 °C). X-ray diffraction confirmed that sample has a single phase, tetragonal structure, and space group P4 mm. SEM analysis confirmed that with increase in concentration of ZnO nanoparticles, the density of microstructure was reduced. Complex impedance analysis disclosed that the material has a multi-Debye type of relaxation processes. It was noted that with the increase in the value of temperature the resistance of grain-boundaries also increased while resistance of grain decreased. Relaxation time was decreased with the rise in temperature for both grain and grain-boundaries. The bulk conductivity of the sample was associated with mobile oxygen vacancies [35].

K. S. Rao et al studied the electrical properties of polycrystalline sample ($Pb_{0.77}K_{0.115}Sm_{0.115}Nb_2O_6$) in frequency range (45 Hz - 5 MHz) at various temperatures (35 °C – 600 °C). The sample was prepared by solid state reaction method. It was concluded from complex impedance spectrum that the sample has a ploydispersive (non-Debye types) nature. The ac and dc activation energies for conduction were estimated from Arrhenius plots [36].

B. Behera et al investigated the structural and impedance properties of the polycrystalline $KBa_2V_5O_{15}$ sample over frequency range (10 KHz - 100 kHz) at different temperatures (200 °C – 375 °C). XRD and SEM were used for phase identification and surface morphology of the sample respectively. The electrical properties of the sample were characterized by complex impedance spectroscopy. Complex impedance spectrum showed that resistance of grains and grain-boundaries were decreased with the increase in temperature resistance. AC conductivity was found to follows the Jonscher's power law [37].

H. Rahmouni et al explained the electrical and dielectric properties of the $La_{0.5}Ca_{0.5-x}Ag_xMnO_3$ ($0 \leq x \leq 0.2$) in frequency range (40 Hz – 10^6 Hz) at different temperature. The sample was prepared by solid state reaction method. It was found that the sample has a semiconductor behavior for all concentration of silver nano-particles. The addition of silver nano particles in the sample was improving the connectivity of grains. A Debye type relaxation was identified for all silver content [38].

R. Chourasia et al explained the impedance of $La_{1-x}Gd_xMnO_3$ (x = 0.1, 0.2, and 0.3) ceramics in frequency range (42 Hz–5 MHz) at various temperatures (50 °C and 300 °C). The

sample was prepared by solid state reaction method. Complex impedance spectrum revealed that grain has the dominant role and a Debye type relaxation in the sample. It was concluded that the sample has a negative temperature coefficient of resistance [39].

T. Acharya et al explained the dielectric and impedance properties of $CoTiO_3$ in frequency range (1 KHz – 10^3 K Hz) at different temperature (25 °C – 400 °C). XRD and SEM were used for crystal structure identification and surface morphology respectively. Dielectric constant as function of frequency was studied by using Maxwell Wagner and Koop's phenomenological model. Complex impedance spectroscopy was used to characterize the electrical properties of the sample. The complex impedance spectrum was depressed with the rise in the. It was observed that the sample has a negative temperature coefficient of resistance just like semiconductors. It was also concluded that the dielectric relaxation in the samples has a non Debye nature [40].

S. R. Mohapatra et al studied the impedance, ferroelectric and magnetic properties of the $Bi_2Fe_4(1-x)Co_{4x}O_9(0, 0.005, 0.01, 0.015,$ and $0.02)$ over a wide frequency range (0.1 KHz – 10^3 KHz) and at different temperature (50 °C – 360 °C). The polycrystalline sample was prepared by solid state reaction method. The complex impedance study of the sample confirmed the presence of multi- Debye type relaxation process in the material. Activation energy was calculated from imaginary part of complex impedance and complex modulus (M'') indicated that the conduction mechanism was due to motion of oxygen vacancies. Magnetic and ferroelectric properties were also improved [41].

A. P. Sakhya et al investigated the dielectric and impedance properties of polycrystalline sample $NdGaO_3$ in frequency range (42 Hz – 5 MHz) at various temperatures (323 K – 593 K). The sample was prepared by sol-gel method. Two relaxation processes was observed which corresponding to grain and grain-boundaries. It was also observed that the sample has a semiconducting nature [42].

Chapter No. 3

Synthesis and Characterization Techniques

3.1 Synthesis of Nanoparticles

There are two approaches for the fabrication of nanoparticles. One is the top down approach which is also known as the physical approach and the second one is the bottom up approach which is known as the chemical approach. In case of top down approach, usually a bulk material is taken and reduces into smaller particles. The major problem of the top down approach is the broad size distribution of particles, surface imperfection, internal stress, and contaminations. The surface imperfection reduces conductivity as a result of inelastic scattering. But in case of bottom up processes a material is build up from the bottom, atom by atom. Bottom up approach is a better technique with the help of which we can obtain nanoparticles having less defects and more homogenous chemical composition [43-44].

3.1.1 Chemical Methods (Bottom up approach)

- Sol-gel technique
- Chemical and physical vapor deposition
- Electro deposition
- Self assembly of nanoparticles
- Laser ablation
- Epitaxial growth

3.1.2 Physical Method (Top down approach)

- Ball milling
- Mechanical deformation
- Arch discharge
- Spray pyrolysis

3.2 Synthesis of Co_3O_4 Nanoparticles

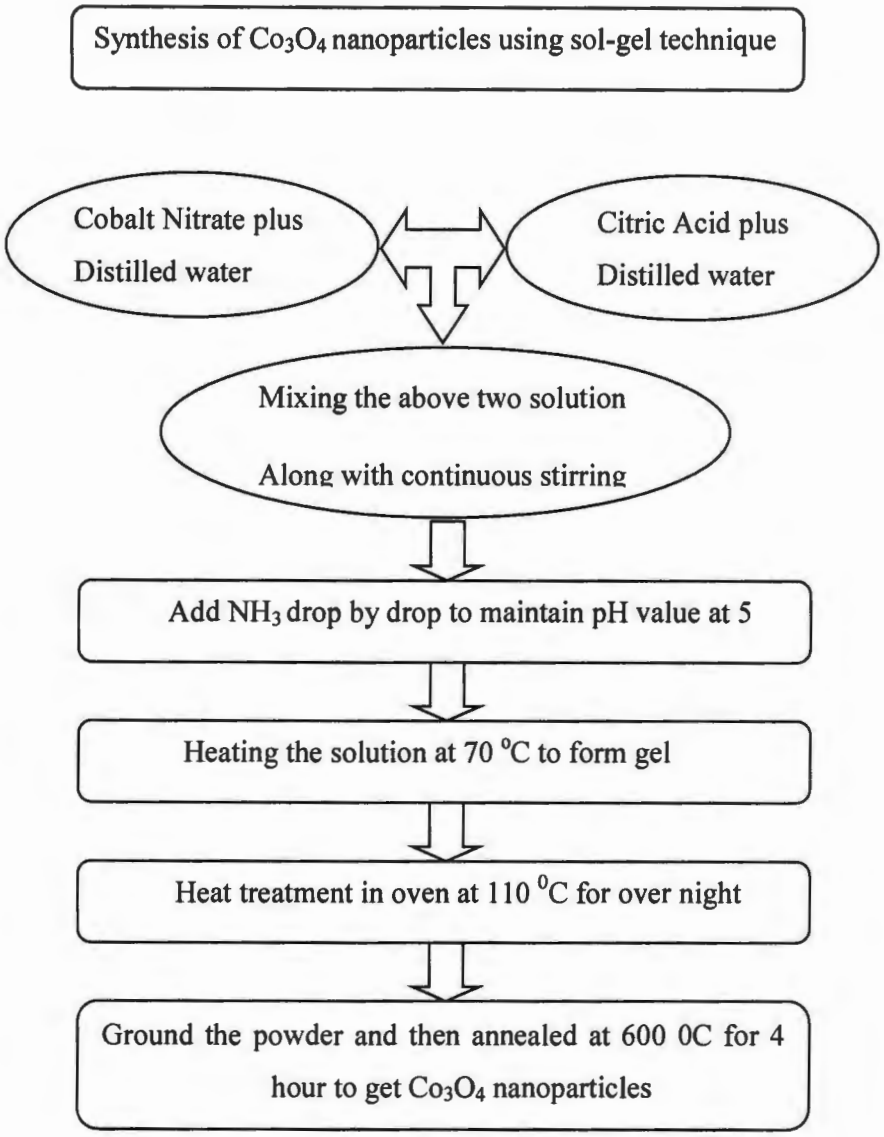

Fig .3.1: The flow chart of synthesis Co_3O_4 nanoparticles.

3.3 Synthesis of Precursor ($Cu_{0.5}Ba_2Ca_2Cu_3O_{10-\delta}$)

The polycrystalline material($Cu_{0.5}Tl_{0.5}Ba_2Ca_2Cu_3O_{10-\delta}$) was synthesized by solid state reaction technique. First we took $Ca(NO_3)_2$, $Cu_2(CN)_2.H_2O$, and $Ba(NO_3)_2.H_20$ in appropriate ratios, mixed them, and ground for two hours in agate mortar and pestle. After that we put the

powder in quartz boat and put them in furnace for 24 hours at 860 ^{0}C. We switched off the furnace for 12 hours to cool down the material. The sample was again grind for two hours and put them in furnace for 24 hours at 860 ^{0}C, and then we grounded the material once again for one hour to get the required precursor $Cu_{0.5}Ba_2Ca_2Cu_3O_{10-\delta}$. The schematic diagram for preparation of precursor ($Cu_{0.5}Ba_2Ca_2Cu_3O_{10-\delta}$) is shown in Fig. 3.2.

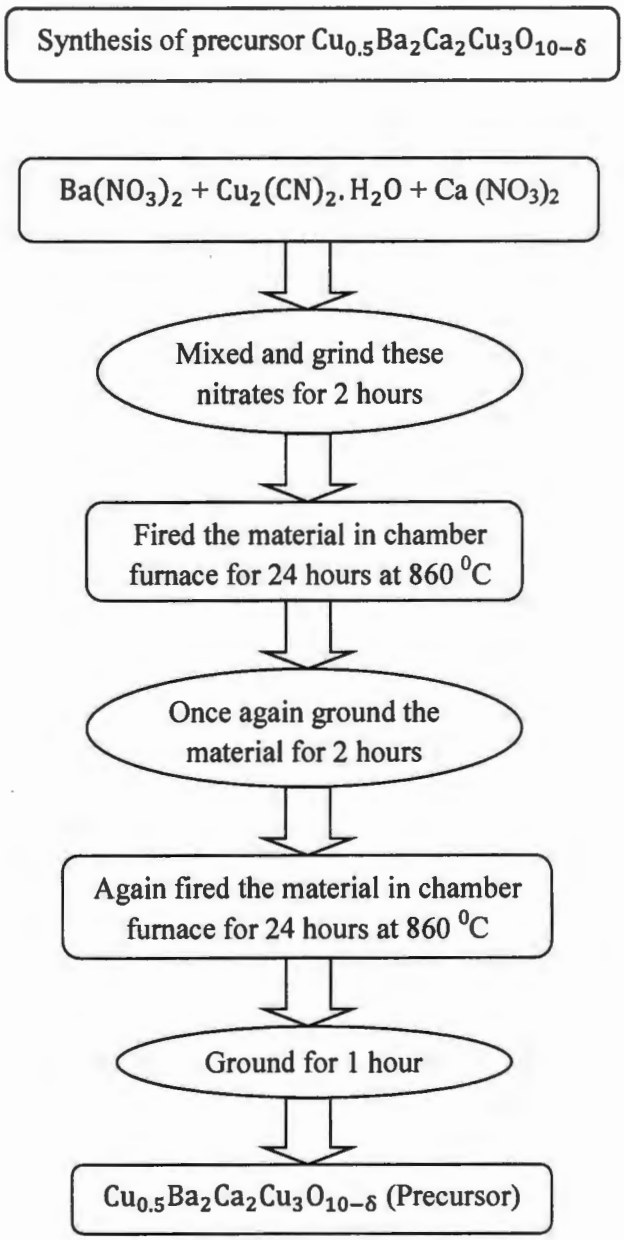

Fig.3.2: Diagram for preparation of $Cu_{0.5}Ba_2Ca_2Cu_3O_{10-\delta}$(precursor).

3.4 Preparation of $(Co_3O_4)_x$/CuTl-1223 Composite

We added Co_3O_4 and Tl_2O_3 in appropriate ratio in $Cu_{0.5}Ba_2Ca_2Cu_3O_{10-\delta}$, pelletized and enclosed in gold capsule, sintered for 10 minute at 860 °C and obtained $(Co_3O_4)_x$/CuTl-1223 nanoparticles superconductor composite as shown in Fig.3.3.

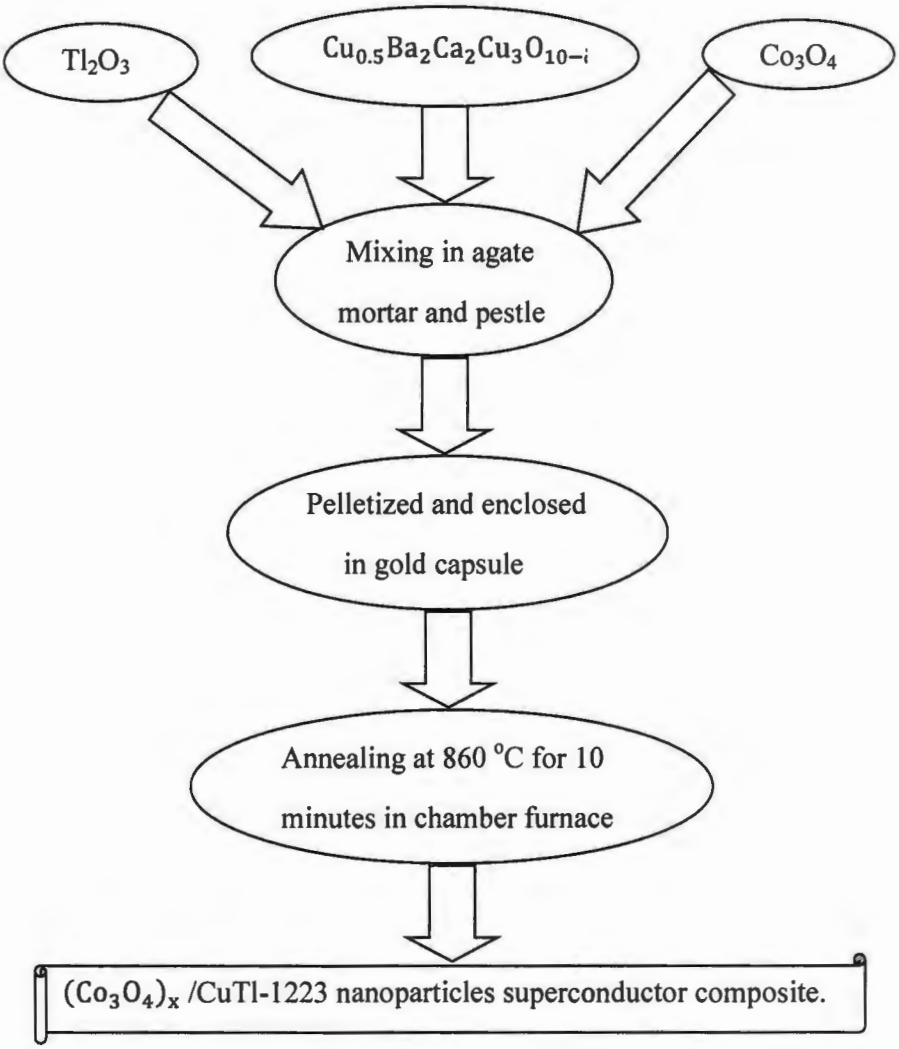

Fig.3.3: The flow chart of the preparation of composite.

3.5 Characterizations

We used the following characterization techniques for the characterization of our samples.

- XRD (X-ray Diffraction) analysis
- R-T (Resistivity versus Temperature) measurements
- SEM (Scanning Electron Microscopy) analysis
- LER meter for complex impedance measurements

3.5.1 X-Ray Diffraction Analysis

It is very important to get information about the structure of material for the practical point of view. With the help of x-ray diffraction we study the structure of the material. X-ray diffraction technique is a nondestructive technique and is a finger print of the material. X-ray diffraction technique is one of the most important experimental technique with the help of which we can get information of the crystal structure of solid material, for the identification of unknown materials, unit cell parameters, orientation of single and polycrystals, crystallite size, crystalline phases, degree of crystallinity, concentrations of impurity, stresses and defects, etc [45].

3.5.1.1 Bragg's Law

X-rays is a type of electromagnetic radiations which have very short wave length (λ) of the order of inter atomic distance. The wave length of x-rays is of the order of atomic distance for solids.

Let us consider a material that has two parallel planes A-Ȧ and B-Ḃ as shown in Fig.3.4. Suppose that these planes have the miller indices (hkl) and interplanar distance d_{hkl}. Suppose a monochromatic beam of x-ray is fall on the planes of atoms. The incident beam of x-rays is scattered by atoms in the planes. Constructive interference will occur only when the path difference between the two rays (1-P-1' and 2-Q-2') is equal to an integral multiple of wavelength (that is $n\lambda$).

$$SQ + QT = n\lambda \tag{3.1}$$

$$SQ = d_{hkl} \sin\theta \tag{3.2}$$

$$QT = d_{hkl} \sin\theta \tag{3.3}$$

Put the values of equation (3.2) and (3.3) in equation (3.1) we get

$$d_{hkl} \sin\theta + d_{hkl} \sin\theta = n\lambda \quad (3.4)$$

$$2d_{hkl} \sin\theta = n\lambda \quad (3.5)$$

Equation (3.5) is called the Bragg's law.

Where

n: 1,2,3…

d_{hkl}: Interplanar spacing

λ: Wavelength of x-ray

θ: Bragg's angle

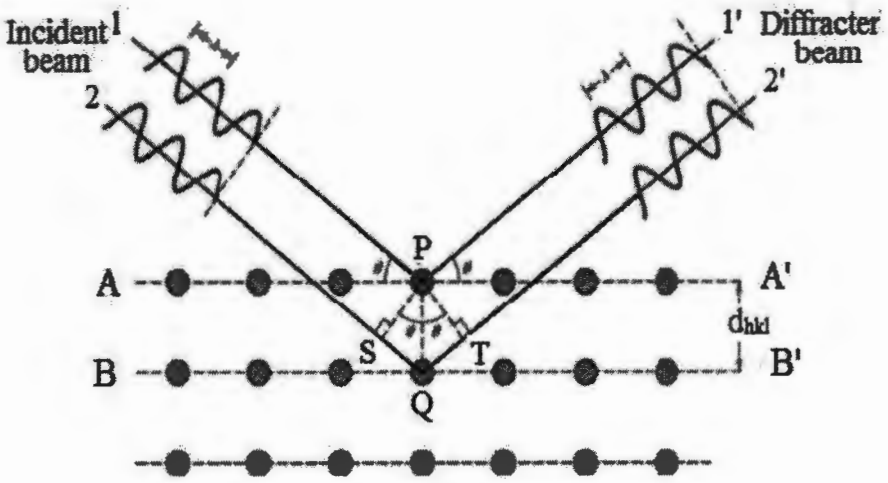

Fig.3.4: The diagram of Bragg's Law and diffraction of x-rays from planes of a crystal [46].

3.5.1.2 Debye Scherrer Equation

Debye Scherrer's equation is one of the most important equations with the help of which we can easily calculate crystallite size of the material. The Scherrer's equation is given as

$$D = \frac{K\lambda}{\beta \cos\theta} \quad (3.6)$$

Where D, K, λ, θ, and β are stand for crystallite size, Scherrer's constant, wavelength of incident x-ray, diffraction angle, and full width at half maxima respectively. The schematic diagram for the calculation of average particle size is given in Fig.3.5.

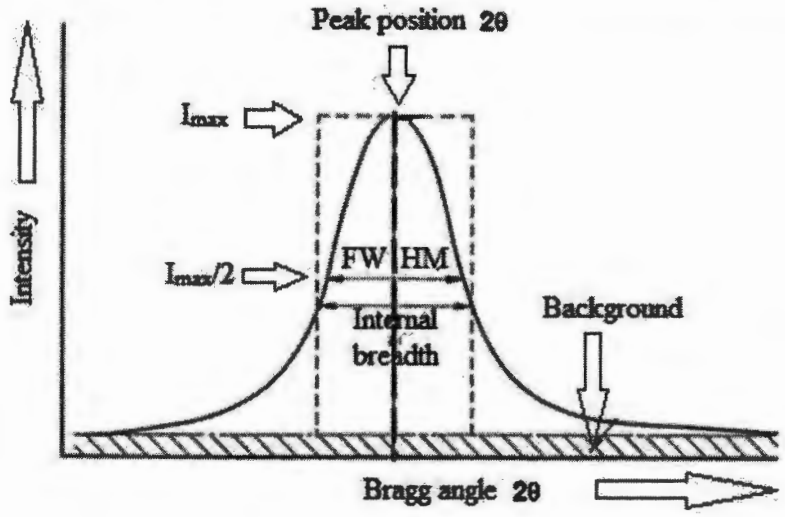

Fig.3.5: The schematic diagram for calculation of grain size [47].

3.5.1.3 Diffractometer

Diffractometer is an instrument which is used for the determination of the angle (θ) at which diffraction take place for powder sample. X-ray Diffractometer consists of x-rays generator, goniometer and electronic circuit panel. It is schematically shown in Fig.3.6. A sample "S" is place on a plate, which can easily rotate about an axis "O" is shown in figure. When a beam of x-rays fall on the sample "S" from the x-ray source "T" intensities of the diffracted x-ray beam are detected by a detector "C". The sample, source of x-rays, and detector are all lays in a plane. The detector moves on a movable carriage, and also rotates about the "O" axis. The angular position of the detector in terms of 2θ is marked on a scale. As the detector moves with a constant speed, a recorder plots the intensity of the diffracted beam as a function of 2θ, where 2θ is the diffraction angle.

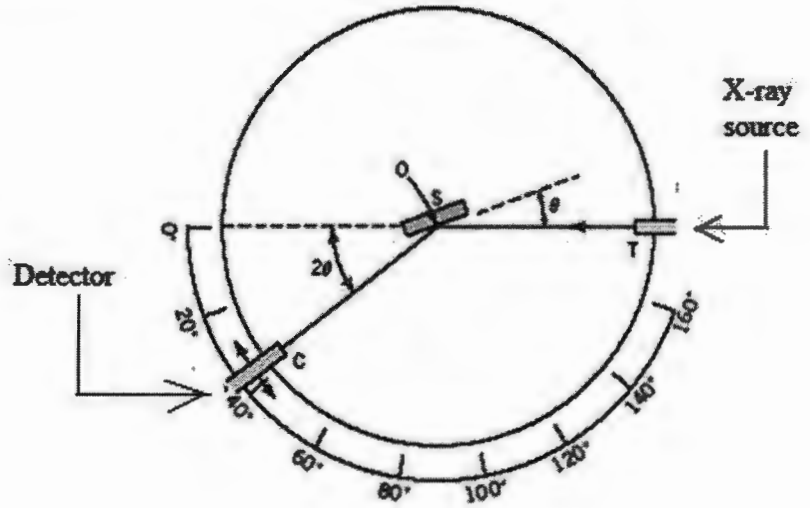

Fig.3.6: Diagram of x-ray Diffractometer [48].

3.6 LCR (Inductance, Capacitance and Resistance) meter

LCR stand for inductance, capacitance and resistance. LCR meter is a device which measure simultaneously inductance, capacitance and resistance of a material. There are two main types of LCR meter that is handheld and bench top. The schematic diagram of LCR meter is given in Fig .3.7.

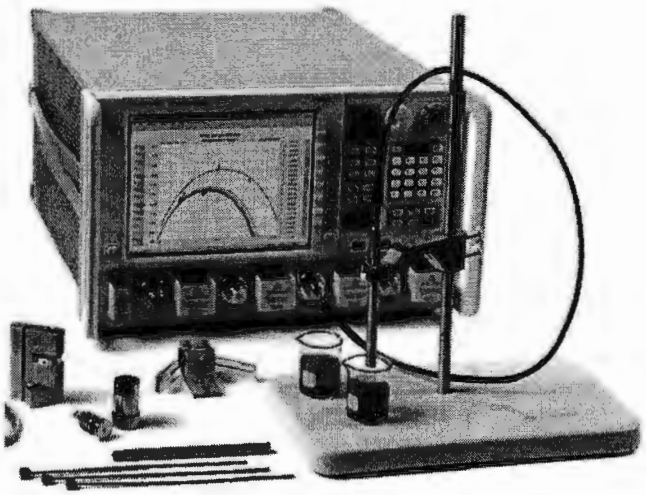

Fig.3.7: The schematic diagram of LCR meter [49].

3.6.1 Handheld LCR meter

Handheld LCR meter has lightweight and operate on a small battery. The advance models of the handheld LCR meter have advance features in which different range of test frequencies and USB connection for transfer of data include. The schematic diagram of handheld LCR meter is shown in Fig.3.8.

Fig.3.8: Diagram of handheld LCR meter [50].

3.6.2 Bench top LCR meter

This is a computer control device. This device gives accurate readings up to 0.01%. Other advantages of the Benchtop LCR meter include DC voltage and sweep capability.

3.7 SEM

Scanning electron microscope is a very powerful device which uses a fixed beam of electrons instead of photons to form a high magnified image of the material under investigation. The basic principle of electron microscope is the interaction between beam of electrons with the sample [51]. In 1924, De-Broglie gives the idea of electron microscope and got the Nobel Prize in 1929. Scanning electron microscopy is a powerful characterization technique for the study of material such is surface morphology, particle size, crystal structure and grain size. Furthermore SEM also use for the characterization of nanostructures. SEM scans the area of the sample and gives the image of the surface on the basis of reflection of electrons from the surface of the material. SEM is a non destructive technique with the help of which we can study the topography of the surface of a sample. SEM produces high resolution three dimensional images of the sample. The different parts of scanning electron microscope are heated filament, electron gun,

electron beam, condenser lens, aperture, objective lens, scanning coils, sample chamber, energy dispersive x-ray detector, backscattered electron detectors, and secondary electron detector. Electronic gun is usually at the top of the column. Electrons are ejected from a filament either by thermionic processes or by applying a strong electric field. The electrons accelerated toward the sample by applying a high potential difference between filament and anode. When the accelerated electrons strike the sample a variety of signals produced such as backscattered electrons, secondary electrons, diffracted electrons, heat and visible light. Secondary electrons and back scattered electrons are use for formation of image of the sample [52]. The various parts of SEM are shown in Fig.3.9. Since SEM is very sensitive therefore it is usually placed on the ground floor of a building, where vibrations negligible to some extent.

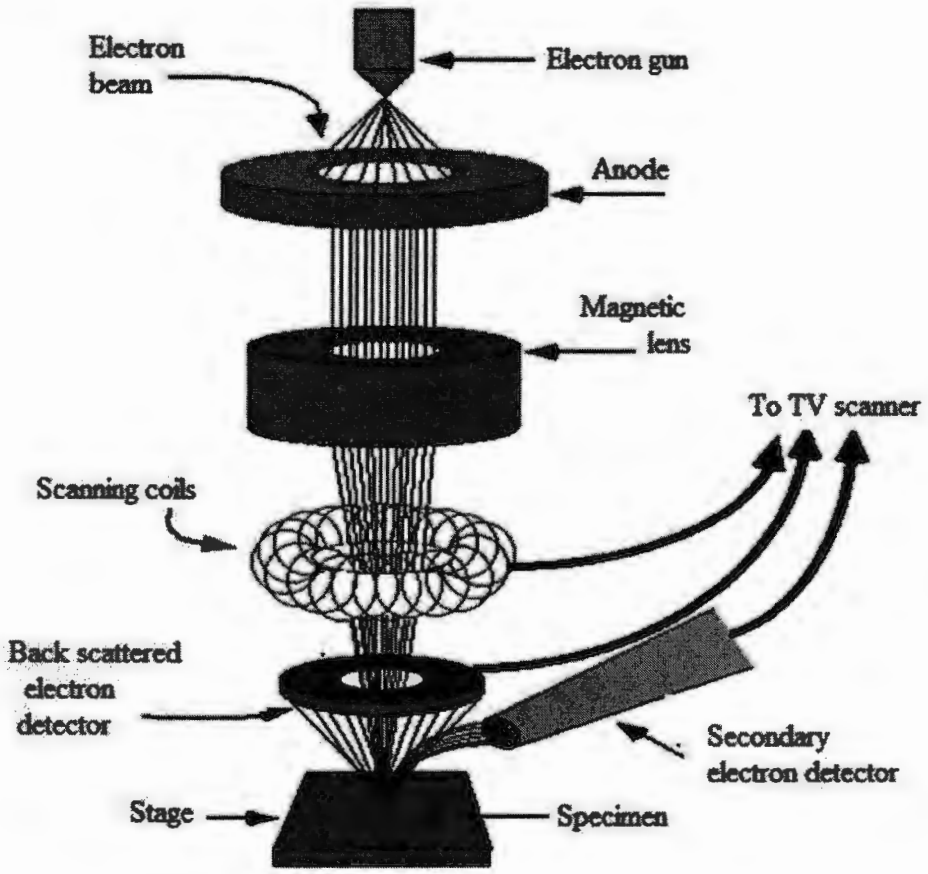

Fig.3.9: SEM diagram [53].

3.7.1 Formation of Image

When incident beam of electron make a collision on the surface of sample different types of signals are produce as shown in figure 3.9. Secondary electrons, auger electrons and

backscattered electrons are investigated to get information about the detail study of the sample [54].

3.7.2 Back Scattered Electrons

When a monochromatic and high energetic beam of electrons fall on the surface of a sample, a part of the incident electrons reflected back from the surface of the sample, which are called back scattered electrons. It is observed that heavy atoms produces more back scattered electrons as compared to light one. So the number of back scattered electrons can be related with the atomic number of the element. Back scattered electrons gives a bright image of the sample with high resolution. Since back scattered electrons reflected back from the surface of the sample therefore these electrons only give information of the upper surface of the sample.

3.7.3 Secondary Electrons

`` Secondary electrons are those electrons which are ejected from the sample, when incident beam of electrons make collision with sample and excite them. The energy of the secondary electrons depends upon the angle between incident beam of electrons and the surface of the sample. If incident beam of electrons and sample are well adjusted then there will be more chances of secondary electrons to eject with high energy that produce a better image of the sample [55].

3.7.4 Auger Electrons

When a high energetic electron ejects inner shell electron vacancy is produce, and atom become unstable. This vacancy can fill by other electrons, which jumps from high energy orbit to lower energy orbit by releasing energy in the form of a photon. The emitted photon is absorbed by outer most electrons and ejects them from their position as shown in Fig 3. 10. The ejected electron is called an auger electron and the phenomenon is known as the auger effect. Auger electrons give us information about the composition and structure of the material under investigation.

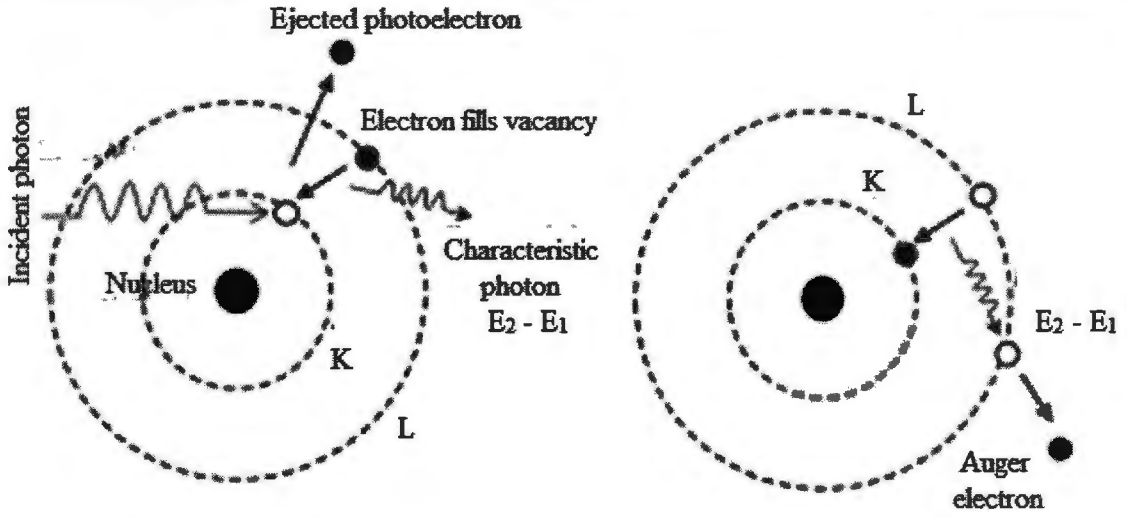

. **Fig.3.10:** The diagram of auger effect [56].

3.8 R-T measurement by Four Probe Method

The simple and basic technique for measurement of resistivity is the "two probe" method. According to Ohm's law the electric current flowing in a conductor is proportional to applied voltage provided the temperature is kept constant. The resistance (R) and resistivity (ρ) of the sample is given by the following relation

$$R = \rho \frac{L}{A} \tag{3.7}$$

Where 'L' and 'A' are the length and cross sectional area of the sample respectively.

The main problem of the two probe method is that if sample has zero resistance the total resistance must be finite, because the resistance of the sample, connecting probe and the contacts between probe and sample are in series. The four probe technique is a better experimental technique. It consists of four probe, two probe are used for current (I) and two for voltage (V) measurement as shown in Fig.3.11. Since no current is passing through the second pair of probe, therefore the contacts resistance not matter. The resistance of the sample between the second pair of probe is given by Ohm's law ($R = V / I$). But in case of a superconductor V= 0 when current (I) is finite and $\rho = 0$ (the current not be very large because for all superconductors there is a critical current I_c, above which the material transform from superconducting state to normal state and resistance again become finite).

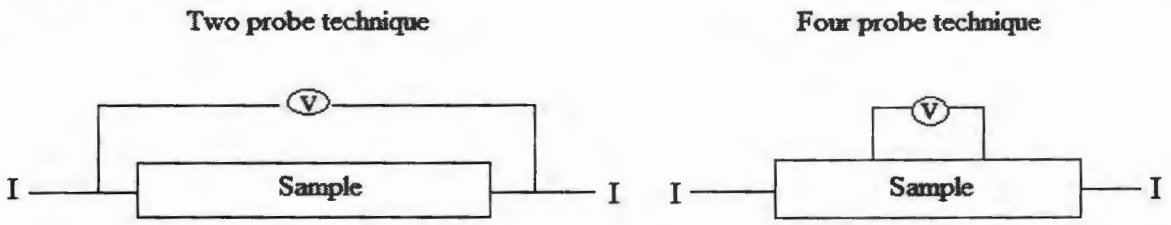

Fig.3.11: The diagram of two and four probe technique [2].

Chapter No.4

Results and Discussion

4.1 X-ray Diffraction Analysis

Fig 4.1 indicates the x-ray diffraction pattern of Co_3O_4 nanoparticles. All the peaks are well defined and well index according to the cubic structure of cobalt oxide nanoparticles. T he presence of sharp peaks shows that the sample has good crystallinity. The average particle size of Co_3O_4 nanoparticles was calculated with the help of Scherrer's equation, which was approximately 71 nm. No any trance of impurity was detected.

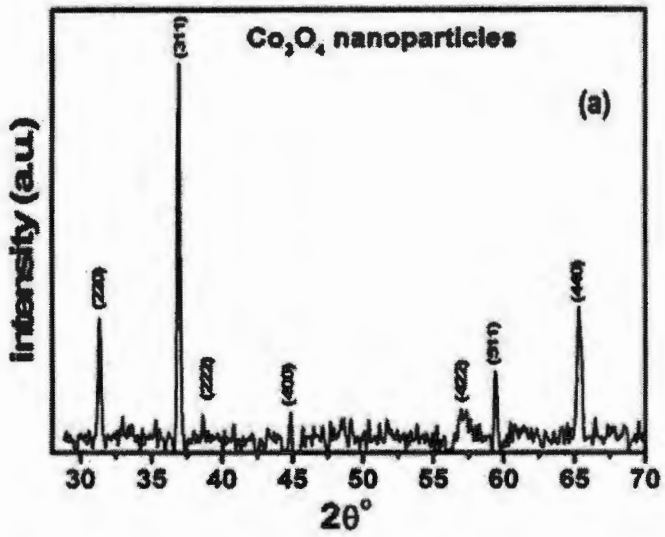

Fig.4.1: XRD graph of cobalt oxide (Co_3O_4) nanoparticles.

The XRD pattern of polycrystalline sample $(Co_3O_4)_x$/CuTl; x= 0 and 1.0 wt.% as shown in Fig.4.2. The x-ray diffraction pattern for x= 0 wt. % is at the bottom of Fig.4.2. Most of the diffraction peaks are well indexed according to the tetragonal crystal structure of CuTl-1223 superconductor. A very low intensity peak of impure phase CuTl-1234 and other unknown impurity also present in the material. After the addition of Co_3O_4 nanoparticles the CuTl-1223 phase remain unaltered which indicates that nanoparticles are disperse at grain boundaries.

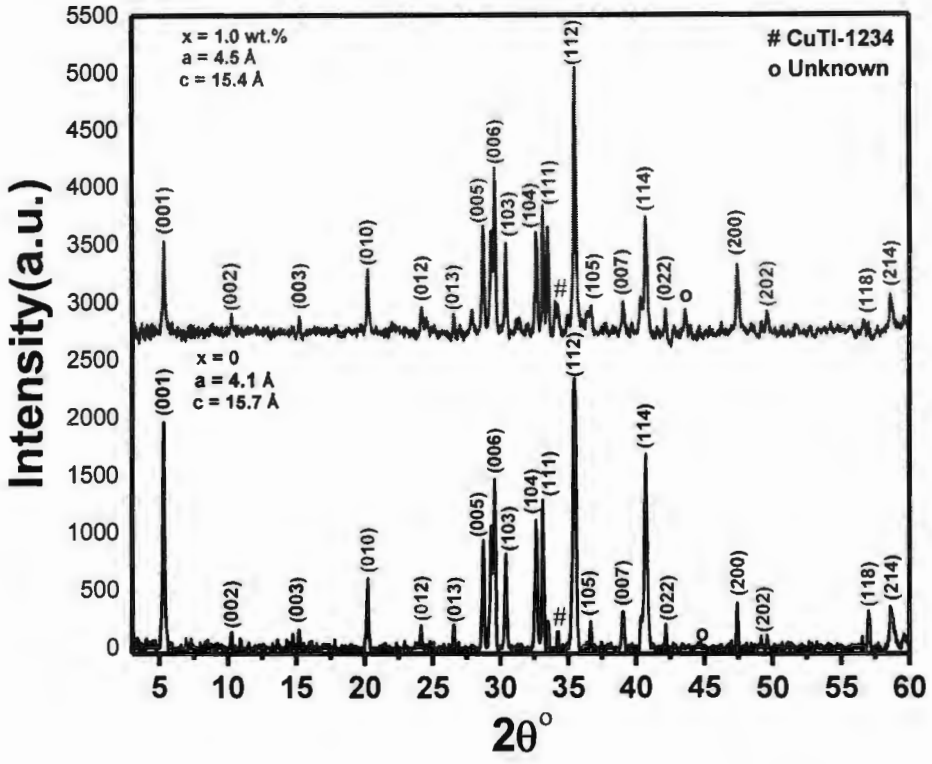

Fig.4.2: The X-ray diffraction pattern of polycrystalline sample of $\{(Co_3O_4)_x$/CuTl-1223; x= 0 and 1.0 wt%.

4.2 R-T Measurements

Resistivity versus temperature measurement of sample of $(Co_3O_4)_x$/CuTl-1223; x= 0.0, 0.25, 0.50, and 1.00 wt.% are shown in Fig.4.3. It is clear from the figure that with addition of Co_3O_4 nanoparticles the superconducting transition temperature, $T_c(0)$ decreases which may be due suppression of superconducting volume fraction. This is because Co3O4 nanoparticles are semiconducting nature, and settle down at grain boundaries. The normal state resistivity of the material enhance with addition of Co_3O_4 nanoparticles, which may be due to enhancement of scattering of charge carriers with impurities.

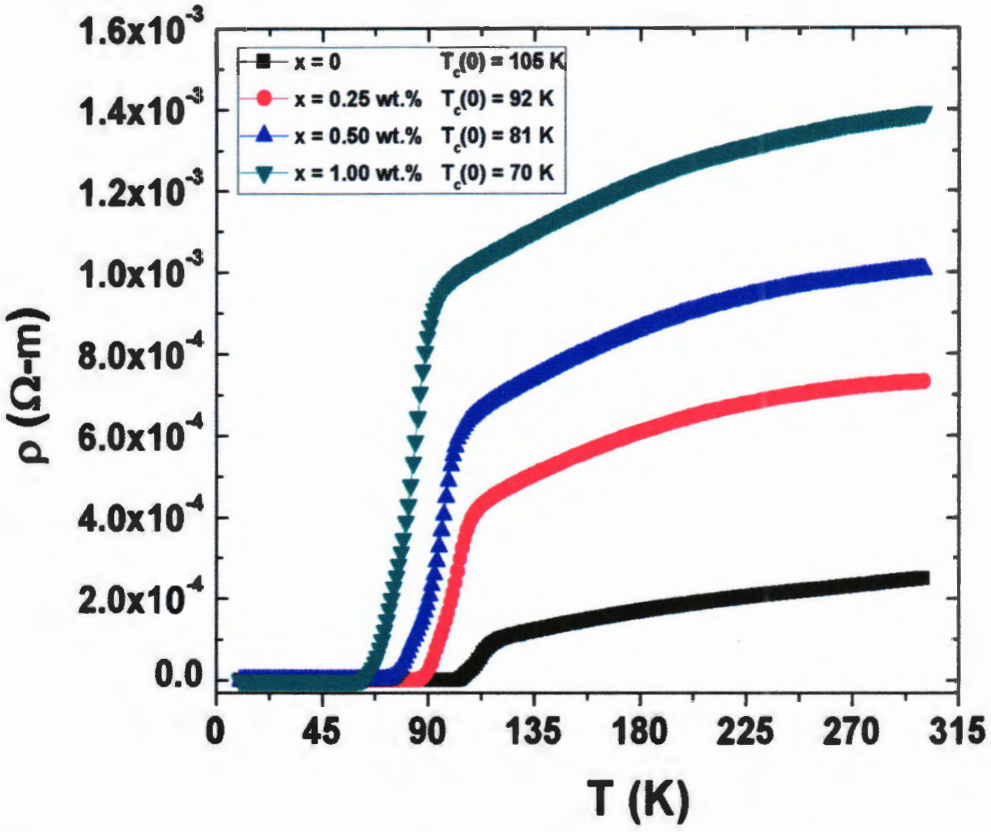

Fig.4.3: Resistivity versus temperature of polycrystalline sample of $(Co_3O_4)_x$/CuTl; x= 0.0, 0.25, 0.50, and 1.00 wt.%.

4.3 Impedance Analysis

The temperature dependence of complex impedance plots of polycrystalline sample $(Co_3O_4)_x$/CuTl-1223; x= 0.0, 0.5, .01, and 2.0 wt. % as a function of frequency range (40 Hz – 10 MHz) are shown in Fig. 4.4 (a- d). It is observed that the height of the spectrum decreases with the increase in concentration of Co_3O_4 nanoparticles in host matrix (CuTl-1223), which may be due to reduction of oxygen vacancies at grain boundaries and enhancement of charge carriers across the grain boundaries. It is also found that with the rise of temperature the intercept of the semicircles with real axes shifted toward the origin, which indicates the decrease in resistance and material has a negative temperature coefficient of resistance behavior just like semiconductors.

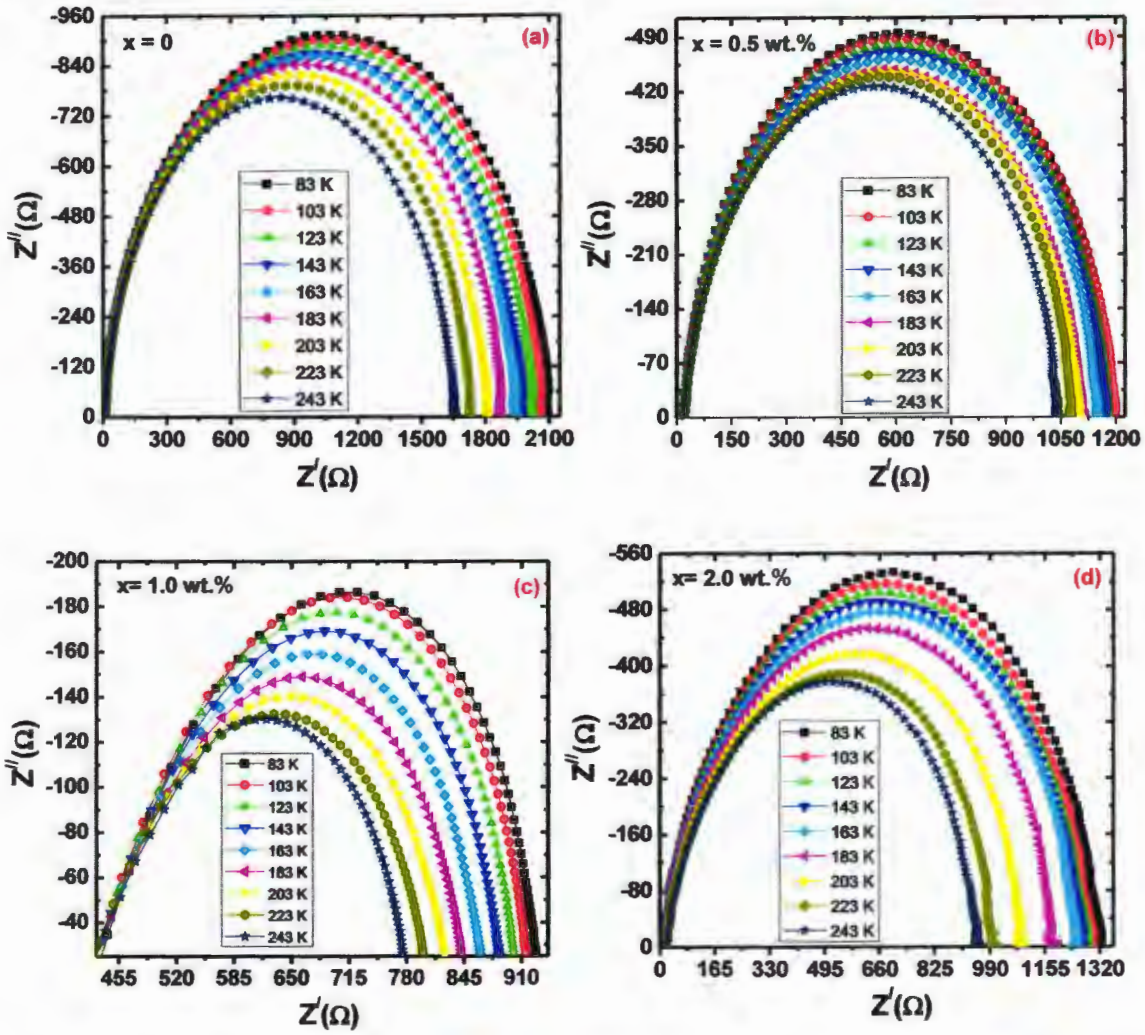

Fig.4.4 (a-d): The temperature dependence of complex impedance plots of polycrystalline sample of $(Co_3O_4)_x$/CuTl-1223; x= 0.0, 0.5, 1.0, and 2.0 wt. % as a function of frequency at different temperature.

Activation energy of the grains and grain-boundaries were calculated by using small polaron hopping model.

$$\frac{R}{T} = A_0 exp\left(\frac{E_a}{k_B T}\right) \quad (4.1)$$

Where

R, T, A_o, E_a, and k_B are resistance, absolute temperature, pre exponential factor, activation energy, and Boltzmann constant respectively

The activation energy of grains and grain boundaries of the sample of $(Co_3O_4)_x$/CuTl-1223; x= 0.0, 0.5, 1.0, and 2.0 wt. % are shows in Fig. 4.5(a-c). The activation energy of grains are 0.88μeV, 1.39μeV, 37.80μeV and 1.58μeV, whereas for grain-boundaries are 201.6μeV, 109.17μeV, 49.21μeV and 122μeV for x= 0.0, 0.5, 1.0 and 2.0 wt.% respectively. Grain-boundaries have high activation energy as compared to grains, which indicates that grains are more conductive than grain-boundaries. The activation energy of grain-boundaries decreases with increase in concentration of Co_3O_4nanoparticales, which may be due to suppression of oxygen vacancies and enhancement of charge carrier across the grain boundaries.

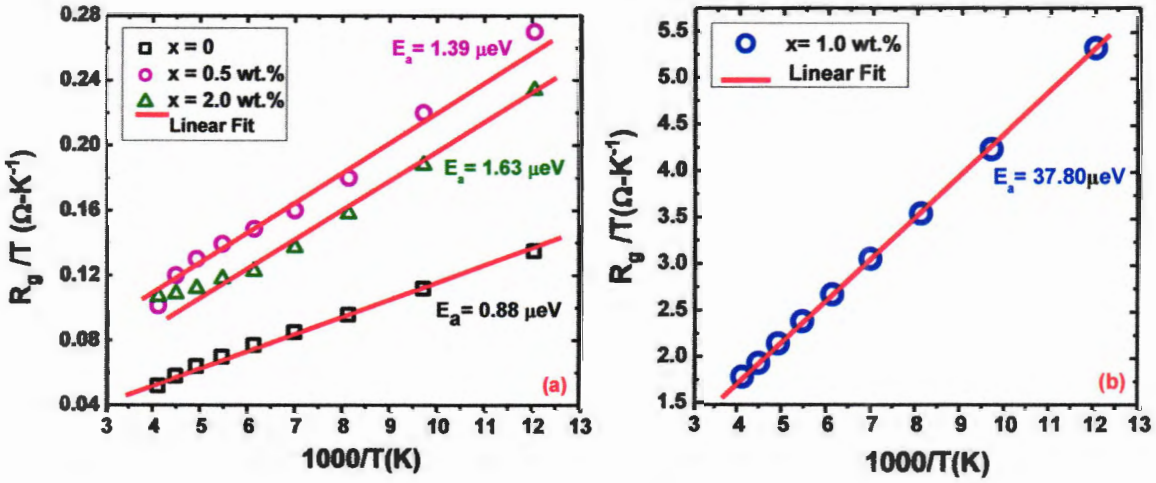

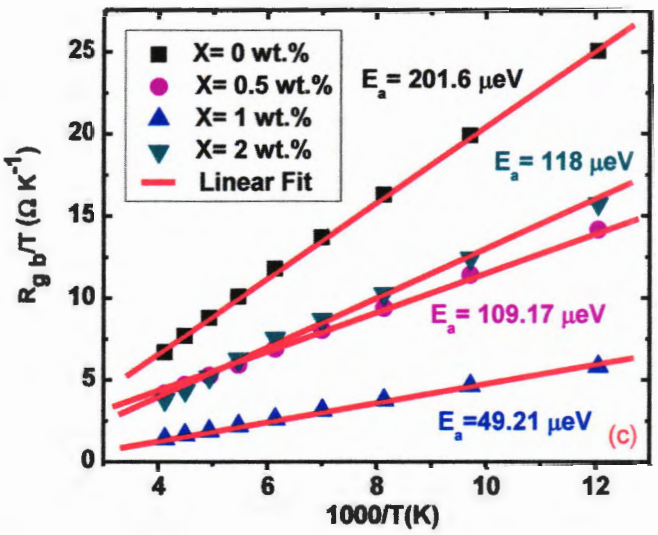

Fig.4.5 (a-c): Activation energy of grains and grain-boundaries of the sample of $(Co_3O_4)_x$/CuTl-1223; x= 0.0, 0.5, 1.0, and 2.0 wt. %.

Fig.4.6 (a-d) shows the real part of impedance (Z′) of the polycrystalline sample of $(Co_3O_4)_x$/CuTl-1223; x= 0.0, 0.5, 1.0, and 2.0 wt. % as a function of frequency range (40 Hz – 10 MHz) at various temperatures (83 K – 243 K).It is noticed that the values of Z′gradually decreases with increase in concentration of Co_3O_4, which may be due to reduction of scattering of charge carriers across the grain-boundaries, and enhancement of conduction process. It has also been observed that Z′has high value at low frequency, which may be due to presence of space charge polarization (interfacial polarization). The value of Z′ decreases with the rise in frequency and finally become constant at high frequency independent of temperature, which may be due to release of space charge polarization as a result of reduction of the barrier across the grain-boundaries. The values of Z′ decreases monotonically with rise of temperature. Insets of Fig.4.6 (a-d) shows that Z′initially has higher value at low temperature (83K) with increase in temperature (83K – 243K) the value of Z′ decreases, which indicates that conductivity enhance with the rise in temperature [57- 61].

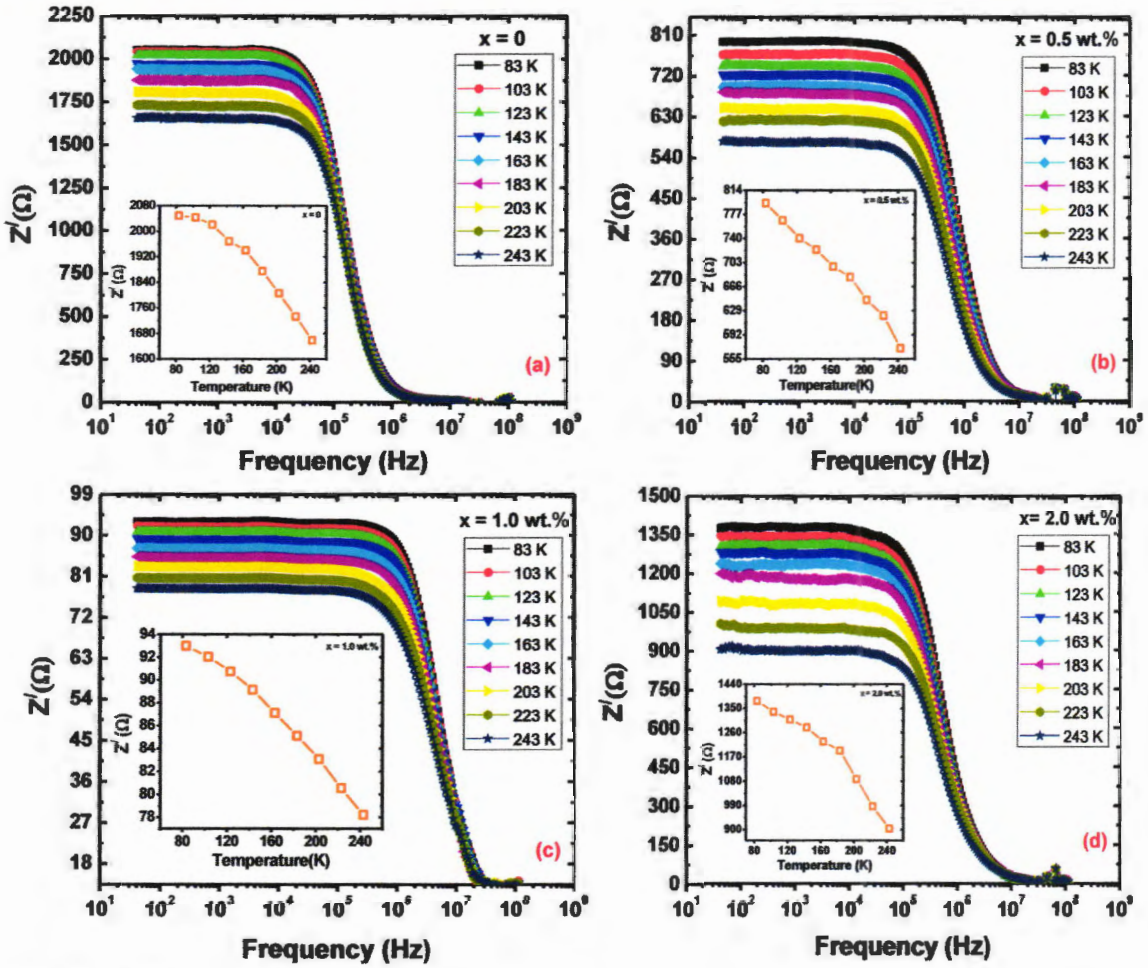

Fig.4.6 (a-d): The real part of impedance (Z') of polycrystalline sample $(Co_3O_4)_x$/CuTl-1223; x= 0.0, 0.5, 1.0, and 2.0 wt. % as a function of frequency range (40 Hz – 10 MHz) at various temperatures (83 K – 243 K).

Fig. 4.6(a-d) shows the imaginary part of complex impedance (Z'') of the sample $(Co_3O_4)_x$ /CuTl-1223; x= 0, 0.5, 1 and 2 wt.% as a function of frequency range from 40 Hz – 10 MHz at various temperatures (83K – 243K). Initially the value ofZ''gradually rise with the rise in frequency, attains a maximum peak value (Z''_{max}), after that the height of the peak decrease with further rise in frequency. It shows that at lower frequency there may be space charge polarizations, which completely vanish at higher frequency [60, 62]. The insets of Fig. 4.6(a-d) shows that the value of decreases with the rise in temperature. The appearance of peak in loss spectrum indicates the existence of relaxation process of the material. The magnitude of $Z''_{(max)}$ decrease with increase in concentration of $(Co_3O_4)_x$ nanoparticles which may be due decrease of resistance. It is also notice that with the increase in concentration of Co_3O_4 nanoparticles the

peaks in the loss spectrum shifted towards the higher frequency side, which may be due to a process with low capacitive effects.

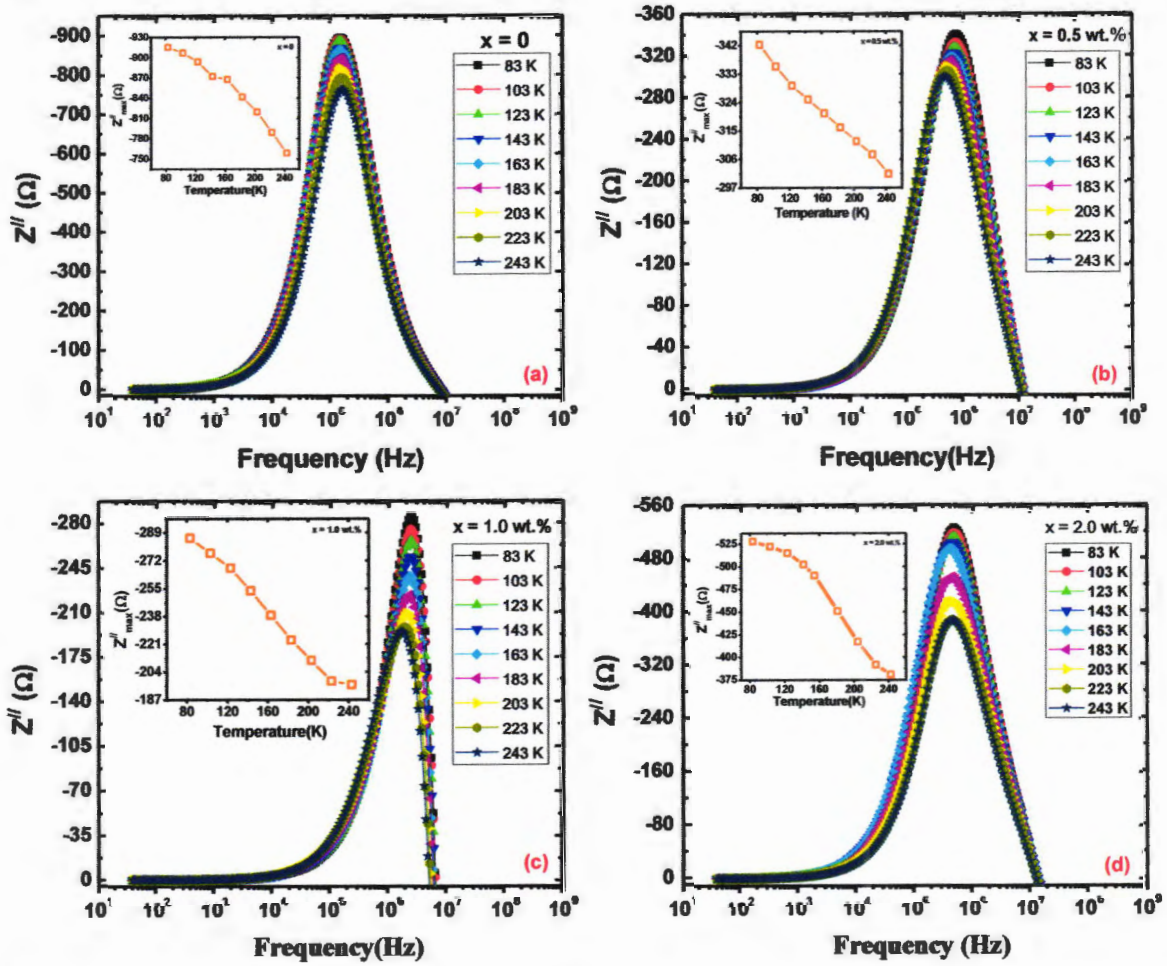

Fig.4.7 (a-d): shows the imaginary part of complex impedance (Z˝) of the sample $(Co_3O_4)_x$ /CuTl-1223; x= 0, 0.5, 1 and 2 wt. % as a function of frequency range from 40 Hz – 10 MHz at various temperatures (83K – 243K).

Fig. 4.7(a-d) shows AC conductivity of the material $(Co_3O_4)_x$ /CuTl-1223; for x= 0, 0.5, 1 and 2 wt.% in frequency range (40 Hz – 10 MHz) at various temperatures (83K – 243K). In the insets of Fig. 4.7(a-d), ac conductivity versus temperature at low frequency (40Hz) is shown. AC conductivity has two regions (i.e. plateau and slop region). In the plateau region conductivity does not depend upon frequency, and known as dc conductivity of material. In the second region, ac conductivity change with frequency. Such a frequency at which ac conductivity start to increase is known as hopping frequency. Ac conductivity change and gradually increase at higher frequencies which indicates a superposition of various transport mechanisms. AC

conductivity increase with the rise of temperature, the dispersive region shifts toward high frequency side. Various types of hopping and mobile charge carriers are include in the transport behavior [63]. With the addition of Co_3O_4 nanoparticles in CuTl-1223 host matrix ac conductivity increase, which may be due to reduction of vacancy at grain-boundaries and increase of charge carriers across the grain-boundaries. The ac conductivity can be interpreted with the help of Jonscher power equation [64].

$$\sigma_{ac} = \sigma_{dc} + A\omega^n \qquad (4.2)$$

Where σ_{ac} is the ac conductivity, σ_{dc} is the dc conductivity, A is a constant which depend upon temperature, and n is an exponent depend on both temperature and frequency.

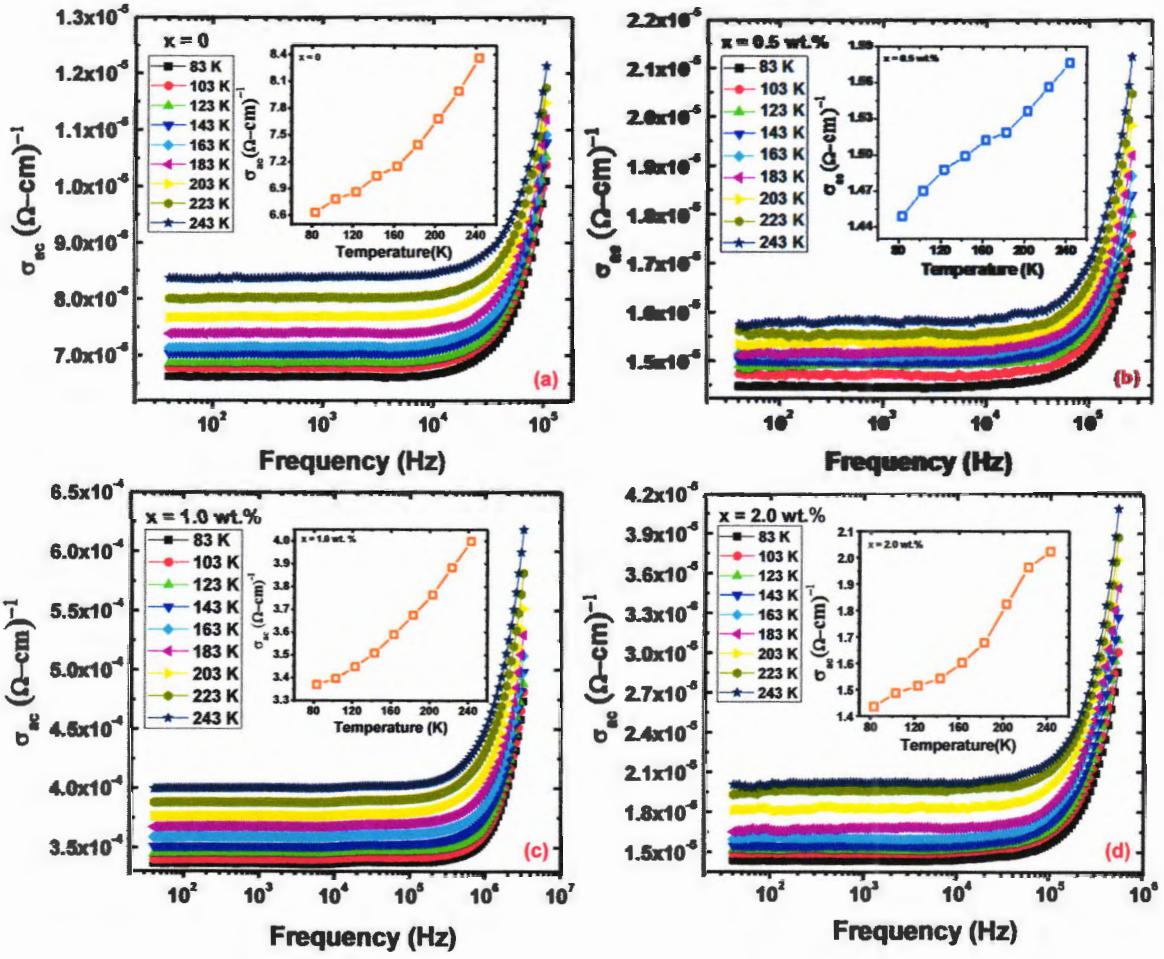

Fig.4.8 (a-d): show AC conductivity of the sample $(Co_3O_4)_x$ /CuTl-1223; x= 0, 0.5, 1 and 2 wt. % in frequency range (40 Hz – 10 MHz) at various temperatures (83K – 243K).

4.4 Conclusion

We synthesized successfully the polycrystalline material of $(Co_3O_4)_x$ /CuTl-1223; x= 0.0, 0.5, 1.0 and 2.0 wt. % nanoparticles superconductor composite with the help of solid state reaction method. XRD technique indicated that the crystal structure of the CuTl-1223 superconductor composite remains unaltered after the inclusion of Co_3O_4 nanoparticles, which provide information that nanoparticles settle down at grain-boundaries. The suppression in superconducting properties is probably due to the semiconducting nature of Co_3O_4 nanoparticles. Complex impedance spectrum indicated that electrical properties control by microstructures. Grain-boundaries have more activation energy as compared to grains, which confirmed that grain-boundaries are less conductive as compared to grains. The decrease in both real and imaginary part of impedance shows thermally activated process in the material.

References

[1] C. Rose and A. H. Rhoderick, "Introduction to Superconductivity", 2nd. Ed, Pergamon Press plc,USA, 3 (1994)

[2] M. Tinhkam, "Introduction to superconductivity", 2nd.Ed, McGraw-Hill, New York, 35 (2004).

[3] D. V. Delft, and P. Kes, "The discovery of superconductivity", Phys. Today, **63**, 38 (2010).

[4] S. Fujita and S. Goday, "Quantum statistical theory of superconductivity", 2nd. Ed, 22 (1996).

[5] https://www.google.com.pk/search?q=resistivity+normal+state,+critical+temperature,&source=lnms&tbm=isch&sa=X&ved=0ahUKEwiqvK7xpMrWAhUIOo8KHe10B8cQ_AUICigB&biw=1366&bih=613#imgrc=TC9PRMyHb9ehOM (29-09-2017).

[6] T. P. Sheahen , "Introduction to high- temperature superconductivity", 1st.Ed, **1**, 22 (1994).

[7] J. Muller, "A15-type superconductors", Phys. Rev. **43**, 641 (1980).

[8] E. Maxwell, "Isotope effect in the superconductivity of mercury", Phys. Rev. **78**, 477 (1950).

[9] J. Gorter, and H. Casimir, "On supraconductivity I", Physica, **1**, 306 (1934).

[10] J. R. Clem, "Granular and superconducting-glass properties of the high-temperature superconductors", Physica C, **153**, 50 (1988).

[11] L. F. Goodrich, and S. L. Bray "High T_c superconductors and critical current measurement", Cryogenics, **30**, 667 (1990).

[12] https://www.google.com.pk/search?q=the+Meissner+effect&source=lnms&tbm=isch&sa=X&ved=0ahUKEwjk4pPIqsrWAhXLNo8KHWjzC48Q_AUICygC&biw=1366&bih=613#imgrc=mtjYS8OqoNUg7M: (29-09-2017).

[13] https://www.google.com.pk/search?q=magnetism+and+magnetic+susceptibility&source=lnms&tbm=isch&sa=X&ved=0ahUKEwiSocn4q8rWAhWIQo8KHV4lDl4Q_AUICygC&biw=1366&bih=613#imgrc=EbrScQrbK1fjRM: (29-09-2017).

[14] Muller, P.Molinié, A. Leblanc,E. Faulques, Z. Ouili, J. C. Jumas, and C. Ayache, "Dissolution of A-15 in Metallic Dichalcogenides", J. Reports Prog. Phys. **43**, 41 (1980).

[15] J. D. Jackson, and R. F. Fox, "Classical electrodynamics", American J. Phys. **67**, 841 (1999).

[16] B. T. Mathias, T. H. Geballe, S. Geller, and E. Corenzwit, "Superconductivity of Nb_3Sn", Phys. Rev. **95**, 1435 (1954).

[17] R. Flukiger, A. Paoli, and J. Muller, "Electronically 'a typical'a 15-type compounds based on chromium and molybdenum", Solid State Comm. **14**, 443 (1974).

[19] L. R. Testardi, "Defects in A-15 superconductors", Cryogenics, **17**, 67 (1977).

[20] F. Abbas, L. E. Davis, and J. C. Gallop."Field solution for a thin-film superconducting parallel-plate transmission line."Physica C, **215**, 132 (1993).

[21] A. B. Pippard "Field variation of the superconducting penetration depth", Proc. R. Soc. **203**, 210 (1950).

[22] L. D. Landau, and V. L. Ginzburg, "On the theory of superconductivity", Zh. Eksp. Teor.Fiz.**20**, 1064 (1950).

[23] https://dc.edu.au/wp-content/uploads/cooper-pair-phonon.png (29-09-2017).

[24] P. Khatri, B. Behera and R.N.P. Choudhary, "Structural and impedance properties of $Ca_3Nb_2O_8$ ceramics", J. Phys. and Chem. Solids, **70**, 385(2009).

[25] https://upload.wikimedia.org/wikipedia/commons/thumb/c/c4/Complex_Impedance. svg /200 px-Complex_Impedance.svg.png (29-09-2017).

[26] Y. Wang, Y. Pu and P. Zhang "Investigation of dielectric relaxation in $BaTiO_3$ ceramics modified with $BiYO_3$ by impedance spectroscopy", J. Alloys and Comp. **653**, 596(2015).

[27] S. kaDash, R. N. P. Choudhary and A. Kumar "Impedance spectroscopy and conduction mechanism of multiferroic $(Bi_{0.6}K_{0.4})(Fe_{0.6}Nb_{0.4})O_3$", J. Phys. and Chem. Solids, **75**, 1376 (2014).

[28] H. Singh, A. Kumar and K. L. Yadav, "Structural, dielectric, magnetic, magnetodielectric and impedance spectroscopic studies of multiferroic $BiFeO_3$–$BaTiO_3$ ceramics", Mater. Sci. and Eng. B, **176**, 540 (2011).

[29] R. Muduli, R. Pattanayak, S. Kumar, S. K. Kar, P. Kumar, S. Panigrahi and R. K. Panda, "Dielectric, ferroelectric and impedance spectroscopic study of Ta_2O_5, Sb_2O_5, and V_2O_5-doped $AgNbO_3$ ceramic", J. Alloys and Comp. **656**, 33 (2016).

[30] D. K. Pradhan, B. K. Samantaray, R.N.P. Choudhary and A. K. Thakur, "Complex impedance studies on a layered perovskite ceramic oxide—$NaNdTiO_4$", Mater. Sci. and Eng, B, **116**, 7 (2005).

[31] S. A. Nedil'ko, I. V. Fesych, O. G. Dzyazko, A. S. Bulachok, S. O. Solopan and T. O. Plutenko, "Synthesis of barium cuprate by secondary induction heating and its electrical properties", Powder Metall. and Met. Ceram. **55**, 5 (2016).

[32] B. B. Mohanty, P. S. Sahoo, M. P. K. Sahoo and R. N. P. Choudhary, "Impedance Spectroscopy of $Ba_5GdTi_3V_7O_{30}$", J. Mod. Phys. **3**, 357 (2012).

[33] Lily, K. Kumari, K. Prasad and R.N.P. Choudhary, "Impedance spectroscopy of $(Na_{0.5}Bi_{0.5})(Zr_{0.25}Ti_{0.75})O_3$ lead-free ceramic", J. Alloys and Comp. **453**, 325 (2008).

[34] P.S. Sahoo, A. Panigrahi, S. K. Patri and R. N. P. Choudhary, "impedance and modulus spectroscopy studies of $Ba_4SrSmTi_3V_7O_{30}$ ceramics", Mater. Sci. Pol. **28**, 4(2010).

[35] Q. K. Muhammad, M. W.aqar, M. A. Rafiq, M. N. Rafiq, M. Usman and M. S. Anwar, "Structural, dielectric, and impedance study of ZnO doped barium zirconium titanate (BZT) ceramics", J. Mater. Sci. **51**, 10048 (2016).

[36] K. S. Rao, P. M. Krishna, D. M. Prasad, J. H. Lee and J. S. Kim,"Electrical, electromechanical and structural studies of lead potassium samarium niobate ceramics", J. Alloys and Comp. **464,** 497 (2008).

[37] B. Behera, P. Nayak and R. N. P. Choudhary, "Structural and impedance properties of $KBa_2V_5O_{15}$ ceramics", Mat. Res. Bull. **43**, 401 (2008).

[38] H. Rahmouni, M. Smari, B. Cherif, E. Dhahri and K. Khirouni, "Conduction mechanism, impedance spectroscopic investigation and dielectric behavior of $La_{0.5}Ca_{0.5-x}Ag_xMnO_3$ manganites with the composition below the concentration limit of silver solubility in perovskites ($0 \leq x \leq 0.2$)", R. soci. Chem. **44**, 10457 (2015).

[39] R. Chourasia, V. Varma, S.Chaurasiya and O. P. Shrivastava, "Crystallographic modeling and impedance studies of gadolinium modified $La_{1-x}Gd_xMnO_3$ (x = 0.1 - 0.3) ceramics", Polyhedron, **121**, 269 (2017).

[40] T. Acharya and R.N. P. Choudhary, "Structural, dielectric and impedance characteristics of $CoTiO_3$", Mater. Chem. Phys. **177**, 131(2016).

[41] S. R. Mohapatra, B. Sahu, M. Chandrasekha, P. Kumar, S. D. Kaushik, S. Rath and A. K. Singh, "Effect of cobalt substitution on structural, impedance, ferroelectric and magnetic properties of multiferroic $Bi_2Fe_4O_9$ ceramics", Ceram. Int. **42**, 12352 (2016).

[42] A. P. Sakhya, A. Dutta and T. P. Sinha, "Dielectric and impedance spectroscopic studies of neodymium gallate", Physica B, **488**, 1(2016).

[43] J. Fujita, T. Kisimoto, M. Morinaga, S. Matsui, and F. Shimizu, "Atomic beam holography for nanofabrication", J. Vac. Sci. Technol. B. **16**, 3855 (1998).

[44] A. Notargiacomo, V. Foglietti, E. Cianci, G. Capellini, M. Adami, P. Faraci, F. Evangelisti and C. Nicolini, "Atomic force microscopy lithography as a nanodevice development technique ", Nanotechnology", **10**, 458, (1999).

[45] C. Giacovazzo, "Fundamentals of Crystallography", Oxford Univ. Press ", 7, 140 (2002).

[46] https://image.slidesharecdn.com/mme323materialsscience-week4-structure of crystalline solides-150118100129-conversion-gate02/95/mme-323-materials-science-week-4-struture -of-crystalline-solids-22-638.jpg?cb=1421575412 (30-09-2017).

[47] https://i.ytimg.com/vi/3Fsr2h2NnAM/maxresdefault.jpg (30-09-2017).

[48] http://slideplayer.com/slide/2437797/8/images/19/Schematic+diagram+of+an+x-ray+diffractometer:.jpg (30-09-2017).

[49] https://bkpmedia.s3.amazonaws.com/photos/889B_left_lrg.jpg (30-09-2017).

[50] https://5.imimg.com/data5/EH/DJ/MY-40366168/lutron-lcr-meter-250x250.jpg (30-09-2017).

[51] B. M. Oliver and J. M. Cage, "Electronic measurement and instrumentation", **35**, 59 (1998).

[52] S. Bertazzo, E. Gentleman, K. L. Cloyd, A. H. Chester, M. H. Yacoub, and M. M. Stevens, "Nano-analytical electron microscopy reveals fundamental insights into human cardiovascular tissue calcification", Nature mater. **12**, 576 (2013).

[53] https://qph.ec.quoracdn.net/main-qimg-362d6d6724b1302ed7821d04c9d2da5e (30-09-2017)

[54] K. Butter, P. H. Bomans, P. M. Frederik, G. J. Vroege, and A. P. Philipse."Direct observation of dipolar chains in iron ferrofluids by cryogenic electron microscopy", Nature mat, **2**, 88 (2003).

[55] J. Cazaux, "Mechanisms of charging in electron spectroscopy", J. Elec. Spect. Rel. Phen.**105**, 155 (1999).

[56] https://wiki.utep.edu/download/attachments/51217142/AESCombined.png?version=1&m-odificationDate=1321071340490&api=v2 (30-09-2017).

[57] I. Coondoo, N. Panwar, A. Tomar, A.K. Jha, and S.K. Agarwal, "Impedance spectroscopy and conductivity studies in $SrBi_2(Ta_{1-x}W_x)_2O_9$ ferroelectric ceramics", Condens. Matter Phys. B **407**, 4712 (2012).

[58] B. behera, P. Nayak, and R.N.P. Choudhary, "Structural and electrical properties of $KCa_2Nb_5O_{15}$ ceramics", Cent. Eur. J. Phys. **6**, 289 (2008).

[59] J. Plocharski and W. Wieczoreck "PEO based composite solid electrolyte containing nasico", Solid. State. Ionics, **28**, 979 (1988).

[60] S. Sen, S.K. Mishra, S.S.Palit, S.K. Das, and A. Tarafdar "Impedance analysis of Pb ($Mg_{1/3}$ $Nb_{2/3}$) $O_{3-0.35}$ $PbTiO_3$ ceramic", J. Alloys. Comp. **453,** 395 (2008)..

[61] B. Tiwari, R.N.P. Choudhary "Frequency–temperature response of $Pb(Zr_{0.65-x}Ce_x$ $Ti_{0.35})O_3$ ferroelectric ceramics: Impedance spectroscopic studies", J. Alloys. Comp. **493**,10 (2010).

[62] J. Fleig and J. Maier "The polarization of mixed conducting SOFC cathodes: Effects of surface reaction coefficient, ionic conductivity and geometry", J. Eur. Ceram. Soc. **24**, 1343 (2004).

[63] Y. B. Tahera, A. Oueslatia, K.Khirounib, and M. Gargouria, "Impedance spectroscopy and conduction mechanism of $LiAlP_2O_7$", Mat. Res. Bull. **78**, 148 (2016).

[64] A. Tabib, N. Sdiri, H. Elhouichet,and M. Férid "Investigations on electrical conductivity and dielectric properties of Na doped ZnO synthesized from sol gel method", J. Alloys Comp. **622**, 687 (2015).